

THE ASTROPHYSICAL JOURNAL 243: 716-735, 1981 February 1
 © 1981. The American Astronomical Society. All rights reserved. Printed in U.S.A.

M83. III. AGE AND BRIGHTNESS OF YOUNG AND OLD STELLAR POPULATIONS

ERIC B. JENSEN¹

Rice University and Air Force Geophysics Laboratory,² Sacramento Peak Observatory³

AND

RAYMOND J. TALBOT, JR.,¹ AND REGINALD J. DUFOUR¹

Rice University

Received 1980 March 21; accepted 1980 August 22

ABSTRACT

By identifying regions free of recent star formation and relatively free of extinction and interpolating between them, we have deconvolved the light of the major stellar populations present in the spiral galaxy M83. We present results in the form of maps of the "old disk" ($t > 10^8$ years), the young light ($t < 10^8$ yr), the distribution of extinction, and the "ages" of the young stellar associations. We have also investigated another deconvolution method which partitions the light of each resolution element in the arms into "young" and "old" components. These methods yield equivalent results for M83.

The "old disk" we derive has substantial azimuthal structure at all radii, consistent with results obtained for other late spirals by other investigators. A weak spheroidal component with $M_V \approx -17.5$, $B - V \approx 0.87$, and $U - B \approx 0.31$ is present, but it dominates the light only in the innermost 500 pc or so. It falls on the color-magnitude relation for elliptical galaxies.

Measurable recent star formation is present in almost every one of our 1.5' (~27 pc) resolution elements located within the inner spiral arms of M83. However, most of the luminosity is confined to clumps, or associations, in aggregates a few hundred parsecs in size. Analysis of the ages and positions of these associations leads to the conclusion that the mechanism responsible for the formation of the stars in the associations must (1) globally trigger formation of massive stars in a well-defined, symmetric two-armed spiral-shaped pattern, (2) locally act in a largely stochastic way over distances of a few hundred parsecs and times of a few tens of million years, and (3) completely terminate after a few tens of million years.

The amount of nucleosynthesis that is implied by our observations, and its radial distribution, is ample to produce the observed gas heavy-element abundances. Unless there is some fundamental error in our measurements of the stellar ages, which is possible if the evolution of massive stars of 4–10 Z_\odot in the H-R diagram is drastically different than 1 Z_\odot stars of the same mass, then corotation of the spiral pattern and the material must lie close to the ends of the inner arms, at $r \approx 180''$, yielding $\Omega_p \approx 67 \text{ km s}^{-1} \text{ kpc}^{-1}$. Several different arguments imply that the star formation we observe greatly favors the production of stars of $\sim 10 M_\odot$ over those of both lower and higher mass when compared with a canonical initial mass function.

Subject headings: galaxies: individual — galaxies: stellar content — galaxies: structure — nucleosynthesis — stars: formation

I. INTRODUCTION

The cause of spiral structure in galaxies and the nature of the interrelationships among the stellar motions, gas flows, star formation, and nucleosynthesis in these galaxies remain among the most interesting and challenging problems in astronomy. A great deal of substantive work on these problems has been accomplished in the last few years, as a result of advances in techniques to obtain and reduce astronomical data and to increased interest in these problems by astronomers (Strom and Strom 1978),

but fundamental understanding of them remains elusive. In order to address some of these problems, we have undertaken a thorough observational study of the bright southern spiral galaxy M83. In the first paper in this series (Talbot, Jensen, and Dufour 1979, henceforth TJD) we presented *UBVR H α* surface photometry of M83, obtained in order to study the history of star formation and structure of this galaxy.

Our goals in our study of M83 were to ascertain the cause or causes of recent ($t < 10^8$ yr) star-forming events, the amount of star formation that is occurring at each position, how the star formation we observe relates to the galaxy's chemical and dynamical evolution, and the amplitude of azimuthal surface-brightness fluctuations in the "old" ($t > 10^8$ yr), smoothly distributed component of the stellar disk. As discussed in TJD, we

¹ Visiting Astronomer, Cerro Tololo Inter-American Observatory, supported by NSF under contract No. AST 74-04128.

² NAS/NRC Resident Research Associate.

³ Operated by the Association of Universities for Research in Astronomy, Inc. under contract AST 78-17292 with the National Science Foundation.

were also interested in making a systematic test of the hypothesis that the propagation of the density wave through the material in the galaxy should leave a wake of young stars aging gradually with increasing distance from the current locus of star formation. To address these questions we have developed procedures for making maps of the luminosity and ages of stars younger than $\sim 10^8$ yr, maps of the distribution of the stellar component older than this, and maps of the extinction. We have derived our maps from the observed *UBV* colors (with some help from the *R* color after correction for $H\alpha$ emission), by the use of a model for the color and brightness evolution of stellar populations similar to those used by other investigators (e.g., Searle, Sargent, and Bagnuolo 1973), the Whitford (1958) law for interstellar extinction, and several plausible assumptions about the spatial distributions of stellar components of various ages.

In this paper we describe the current state of development of these procedures and present results for M83. The remainder of this section summarizes the previously published observational material and briefly describes the assumptions we have used for its interpretation. The procedures we have used to extract each of the components of the galaxy, and the results for each component, are presented in the following sections: II (spheroid), III ("old disk"), and IV ("cluster"). Section V, labeled "Interpretation of Results," compares the recent star formation deduced in § IV with that predicted by simple models of galactic evolution and to some simple "predictions" of the density-wave hypothesis. Section VI is simply a summary of the results and conclusions collected from the previous sections. The first-time reader of this somewhat complex work is advised to finish the introduction, skim §§ II, III, and IV, and read § V carefully before returning, if he has the stamina, to consider the myriad of technical details contained in our discussions of the deconvolution of the spheroid, disk, and cluster components.

a) Observational Material

The photographic passbands used in TJD were $u = 103aO + UG - 2$, $b = 103aO + GG385$, $v = 103aD + GG495$, and "*r*" = 098 + RG610. To transform these to the Johnson *UBVR* system, the following color equations were adopted:

$$U = u \quad (1)$$

$$B = b + 0.039 - 0.052(b - v) \quad (2)$$

$$V = v - 0.066 + 0.086(b - v) \quad (3)$$

$$R = -0.33 + 1.43(v - r). \quad (4)$$

The transformations to *B* and *V* were obtained by adopting the average of the coefficients derived by Anthony-Twarog, Twarog, and McClure (1979), Stetson and Harris (1977), Harris and Harris (1977), and Menzies (1972). While these corrections are small, they are not

completely negligible. No suitable transformation equation to transform the 098 + RG610 passband to the Johnson *R* was found in the literature; our transformation was deduced by calculating the effective wavelengths of the photographic bandpass and the Johnson *R* bandpass for a mix of late stellar populations. Note that this transformation cannot be said to be well established and is large since the photographic passband is not a particularly good match to Johnson *R*. Our "*r*" passband and $H\alpha$ passband data have been appropriately normalized and subtracted in order to remove $H\alpha$ and [N II] from the derived *R* and to remove red continuum from the derived $H\alpha$.

The 4 m plates were scanned with a 40 μm square aperture, yielding pixels 0''.744 on a side. In this paper, we utilize 2×2 averages of these pixels, hence our pixel size is 1''.488 corresponding to 27 pc at the galaxy, using a distance of 3.75 Mpc (de Vaucouleurs 1979). We follow TJD in continuing to use a value $A_v = 0.28$ mag for the extinction in our galaxy, yielding $E(B - V) = 0.08$ and $E(U - B) = 0.06$. Brightnesses and colors corrected by these amounts have zero subscripts.

b) Assumptions for the Deconvolution of Different Stellar Populations and Extinction

The maps and most of the discussion presented in this paper are derived from the following network of assumptions concerning the stellar populations of spiral galaxies:

1. Throughout most of a galaxy such as M83, now and through much of the past, star formation has occurred with an initial mass function (IMF) which can be characterized by a power law similar to the Salpeter IMF applicable to the solar neighborhood, and with roughly solar metallicity:

$$\psi(m) \propto m^{-1.35}, \quad (5)$$

where $\psi(m)dm$ is the fraction of mass in the interval m to $m + dm$. By "similar," we mean to include all power laws for which the integrated cluster colors are dominated by the top of the main sequence and the giant branch, and hence are nearly independent of the power-law exponent. This includes at least the range $1.1 \leq \text{exponent} \leq 2.2$ (Searle *et al.*). Consequently, stellar cluster evolution tracks such as those of Dixon, Ford, and Robertson (1972), Tinsley (1972), and Searle *et al.* may be applied, after transforming to *UBVR* using tables from Johnson (1966), Morton and Adams (1968), Lee (1970), and Greenstein, Neugebauer, and Becklin (1970). The cluster track we use in this paper is one we have calculated (cf. Davis 1979), employing, specifically, the following IMF:

$$\psi(m) = 0.272 m^{-1.35}, \quad 60 M_\odot > m \geq 1.8 M_\odot \quad (6a)$$

$$\psi(m) = 0.175 m^{-0.60}, \quad 1.8 M_\odot \geq m > 0 M_\odot, \quad (6b)$$

where $\psi(m)dm$ is the fraction of mass contained in the interval m to $m + dm$ and $\int_0^\infty \psi(m)dm = \int_0^{60} \psi(m)dm = 1.0 M_\odot$. The coefficients are chosen so that $\psi(m)$ is continuous at $m = 1.8 M_\odot$. The choice of the low-mass exponent = -0.60 fits the solar neighborhood data

adequately and gives a function whose total mass does not diverge as $m \rightarrow 0$ (Talbot and Arnett 1975). Our cluster track is essentially indistinguishable in UBV from those of Tinsley (1972) and Searle *et al.* since all are based on stellar tracks by Iben (1965, 1966, 1967), Stothers (1963, 1964, 1966), and Stothers and Chin (1968). There are significant differences, however, between our cluster track and that of Dixon, Ford, and Robertson (1971) which were based on the high-mass stellar tracks of Robertson (1971, 1972).

2. Interstellar extinction in M83 obeys the Whitford (1958) law. We adopt $E(U - B) = 0.72E(B - V)$, $E(V - R) = 0.80E(B - V)$, and $R = A_V/E(B - V) = 3.3$, following Johnson (1968).

3. After subtraction of a central spheroid from the light of the galaxy, the integrated light of each pixel in the galaxy consists of light from two components having different spatial distribution and different color properties. The first is the "old disk," "smooth disk," or simply "disk;" it is here defined as the light from all stars older than $\sim 10^8$ yr (intended to roughly approximate the time between passages of the material through a spiral arm), and assumed to be smoothly varying in surface brightness and color. The second component is the light from a single star-forming event of a unique age less than $\sim 10^8$ yr if there is evidence for such; otherwise the pixel is set to blank. This component will be called the "young" component or "cluster" component since generally this light will come from a cluster or association of young stars.

II. SPHEROIDAL COMPONENT

For the preceding network of assumptions to be realistic, it is necessary that the galaxy light not be confused by the presence of stellar components in addition to our "old disk" and "cluster" components. For this reason, we have sought to fit and subtract from our data the light of the spheroid or bulge component of M83. As discussed in TJD, such a component appears to dominate the light in an annular ring between $\sim 10''$ and $40''$ in radius (0.18–0.72 kpc). It is identifiable as a spheroid by the circularity of the isophotes in the $10''$ – $40''$ range, except for irregularities obviously resulting from dust lanes and small regions of recent star formation. These near-circular isophotes are in striking contrast to those of the bar-dominated component farther out. This region of the galaxy also yields a good fit to an $r^{1/4}$ law, albeit over only $\sim 2\frac{1}{2}$ mag range along the minor axis and only $\sim 1\frac{1}{2}$ mag range along the major axis. The $r^{1/4}$ region is bounded on the inside by the ultraviolet-rich nuclear region (Evans 1956; TJD) and on the outside by the bar along the major axis and the disk along the minor axis. These bar and disk components share an exponentially declining surface brightness with approximately the same scale length, and their colors suggest that they are both comprised of the same stellar population. We assume that they are largely confined to the central plane of the galaxy, unlike the spheroid.

In order to measure the light from the spheroid, we have constructed a radial profile using the azimuthal

average of all pixels for inner radii, but using pixels only along the minor axis for radii $r > 23''$ where the bar begins to dominate the major-axis profile. This profile is shown in Figure 1. We have chosen to fit these data with a function consisting of the sum of an $r^{1/4}$ law and an exponential, fixing the exponential e-folding scale length $r = 237''$ by using the red pixels at large radii in Figure 7b of TJD. The result for the spheroid is

$$V = 19.50 + 8.327[(r/18''.37)^{1/4} - 1]; \quad (7)$$

this is shown as a dashed line in Figure 1. The extrapolated central surface brightness of the exponential derived from this fit is $V = 20.59$. The data in Figure 1 and equation (5) are uncorrected for extinction from the Milky Way. For this spheroid, $M_V = -17.20$, or -17.48 corrected for galactic extinction, assuming a distance of 3.75 Mpc. Unfortunately, the dust and young stars much more seriously contaminate the B and U profiles in the critical $10'' \leq r \leq 40''$ region, making our estimates of the color of the spheroid somewhat uncertain. We nonetheless obtain $B - V = 0.95 \pm 0.05$, $U - B = 0.37 \pm 0.05$ (estimated 50% uncertainties). It is interesting that these colors, corrected by $E(B - V) = 0.08$, $E(U - B) = 0.06$ for galactic extinction, fit well with the color-magnitude

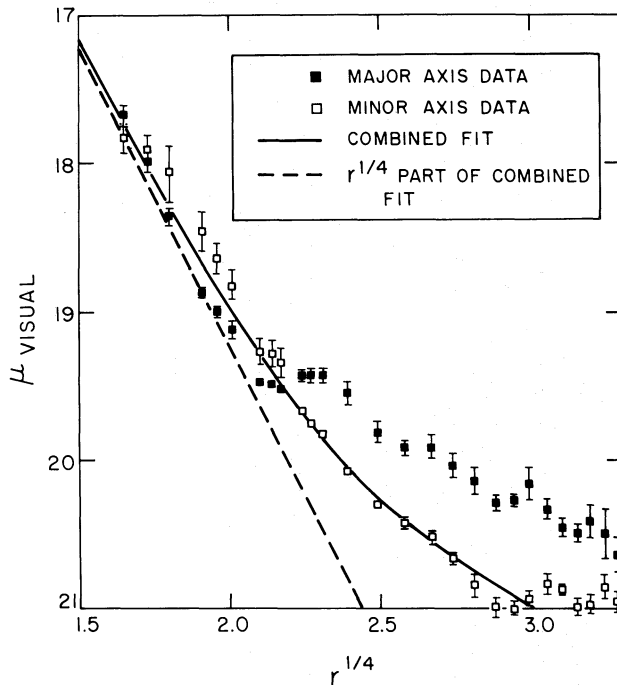


FIG. 1.—The V surface brightness of the inner region of M83 fitted to the sum of a de Vaucouleurs $r^{1/4}$ spheroid and an exponential disk. Pixels along the major axis (which lies along the bar) are plotted as filled symbols, while pixels along the minor axis are plotted as empty symbols. Each point plotted is the average of all pixels in a polar bin $5''$ by $22.5''$ in the plane of the sky; the circular symmetry interior to $r^{1/4} = 2.1$ strongly suggests the existence of a true spheroidal component. The combined spheroid plus exponential fit is shown as a solid line, while the fitted spheroid alone is shown with a dashed line. The fit employed was made to the minor axis points only.

relation for elliptical galaxies (Visvanathan and Sandage 1977; Sandage and Visvanathan 1978).

We have subtracted from our data the spheroid expressed by equation (5) using the colors $B - V = 0.95$ and $U - B = 0.37$. As it turned out, this did not have a substantial effect on the color distribution in the inner part of the galaxy, since the "disk" color within $\sim 60''$ of the nucleus is approximately the same as the spheroid.

III. OLD DISK COMPONENT

We designate the "old disk" (or "smooth disk") to be the stellar component which would be left if we could strip away the spheroidal stellar component, all of the dust in the galaxy, and all of the young stars whose light dominates the arms, especially in the blue, and which generally exhibit a very patchy spatial distribution. Within the context of the density-wave picture, we can draw a very specific theoretical boundary between the "young" and "old" disk stars, the "young" stars being all those that have formed since the last passage of the "crest" of the density wave through the particular region of the galaxy.

The technique we have developed to deconvolve the "old disk" component from the young stellar component and the extinction consists simply of identifying essentially uncontaminated "old disk" regions throughout the galaxy and interpolating between them. The next paragraph describes how we selected the "old disk" regions, while the exact steps involved in producing our map of the "old disk" are described in the following paragraphs and illustrated in Figure 2 (Plate 12).

Star formation and extinction in M83 are so ubiquitous that uncontaminated "old disk" regions are not obvious at first glance. However, careful inspection of the intensity and color maps and azimuthal and radial profiles disclose numerous regions which appear to be essentially uncontaminated. These regions are distinguished by the following properties:

i) Smooth surface brightness and intermediate color. Individual bright young stars or clusters are lumpier than these smooth regions, and bluer. Dust lanes and clouds are filamentary in appearance, and *redder* than the smooth patches;

ii) The smooth regions, at a given radius, are of essentially constant color, consistent with the idea that they are representative of a homogeneous unobscured stellar population;

iii) Some of these smooth regions are located just inside the prominent dust lanes on the insides of the bright arms; they are just 0.75 mag brighter than the adjoining dust lane. If the dust is concentrated in the central plane of the galaxy, this is most simply explained if the dust in the lane is optically thick and is completely obscuring the half disk below it, and the adjoining smooth patch is suffering essentially no extinction.

In practice, we have used property (i) to *identify* "old disk" regions, and properties (ii) and (iii) to confirm our identifications. The "old disk" regions we identify are of constant color at a given radius, but we find a radial color

gradient inside the radius corresponding to the ends of the inner arms. We therefore have approximated the "old disk" color by the following ramp plus constant function (the colors are not corrected for galactic extinction).

$$\begin{aligned} (B - V) &= 1.14 - 0.43(r''/150), \\ (U - B) &= 0.59 - 0.41(r''/150), \\ 0 \leq r'' &\leq 150 \end{aligned} \quad (8)$$

and

$$(B - V) = 0.71, \quad (U - B) = 0.18, \quad r > 150''. \quad (9)$$

We have used our originally identified "old disk" regions only to define this color distribution. In the algorithm that produces a complete map of the "old disk," we use as input only the color distribution defined by equations (8) and (9). The following paragraph describes the algorithm; in order to make it intelligible, the reader is urged to refer to Figure 2 at this time.

First, we subtracted from the V picture (panel A of Fig. 2) the spheroid component whose computation we described in the preceding section (panel B). Next, we selected all those pixels whose colors lie within ± 0.05 of the values defined by equations (8) and (9). The result is displayed in panel C of Figure 2: we have succeeded in extracting the little smooth regions from the interarms, along with a scattering of additional pixels of various brightnesses, many in the arms or in the dust lanes. Panel D displays how these discrepant pixels were eliminated, by replacing each pixel with the mean of those in a five by five pixel box surrounding it, *retaining only those pixels* in the box within two standard deviations of the mean. This procedure effectively eliminated isolated and discrepant pixels from the map, leaving only contributions from pixels lying in smooth regions. Interpolation of the resulting data through adjoining regions, mainly arms and dust patches, was performed after a transformation of the map to a polar coordinate system in the plane of the galaxy, assuming a galaxy inclination of 24° to the plane of the sky. The smoothed x, y data shown in panel D were collected into r, θ bins of size $r = 15'', \theta = 6^\circ$ (panel E, left). This binning had the effect of smoothing the data further. Additional smoothing and interpolation into blank, r, θ pixels was achieved by applying the same smoothing algorithm used to produce panel D, only with 3×3 averages (panel E, right). The r, θ plots in panel E are displayed with the center of the galaxy at the left and θ (measured counterclockwise from the major axis at position angle 45°) increasing downward. Finally, the data were transformed back to x, y coordinates, interpolating among adjacent r, θ pixels to calculate each x, y pixel. The result of this procedure, adopted as our best estimate of the V flux of the "old disk," is displayed in panel F. The same procedure as illustrated here to derive the V flux of the old disk was applied to the $B - V$ and $U - B$ colors as well; the resulting color maps were combined with the V map in panel F to produce maps of B and U .

Figure 3 presents for comparison the radial profiles of

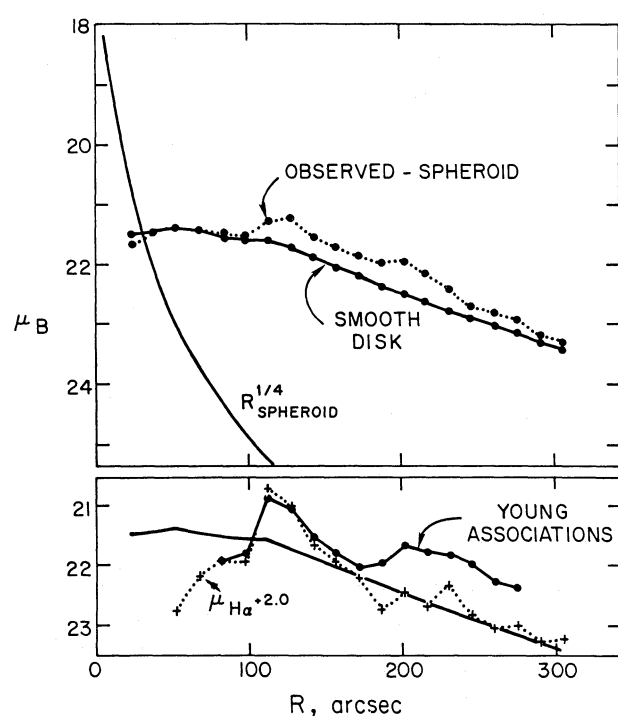


FIG. 3.—The upper panel displays the radial profile of several components of the light of M83: the spheroidal component whose derivation is illustrated in Fig. 1 and discussed in § II, and the smooth “old disk” component whose derivation is illustrated in Fig. 2 and discussed in § III. Also shown is the observed B profile after subtraction of the spheroid. The solid line in the lower panel is the smooth “old disk” component, the same as in the upper panel. Also shown in the lower panel are the radial profiles of the H α flux (shifted by 2.0 mag) and of the blue luminosity of the young “clusters,” as derived and corrected for extinction in § IV.

the blue surface brightness of the old disk and of several other components of M83. In the top panel the $r^{1/4}$ law spheroid is shown together with the observed surface brightness after subtraction of the spheroid and the derived smooth “old disk.” The latter two and the other surface brightnesses in the lower panel are averages around circles in the plane of the galaxy using an inclination of 24° derived from the apparent ellipticity of the outer isophotes. Beyond $r = 100''$ the profile of the smooth “old disk” becomes very nearly an exponential over $\sim 1\frac{1}{2}$ e-folding scale lengths of $r = 237'' = 4.26$ kpc (at 3.75 Mpc). This is larger than the e-folding length derived in TJD from the profile of all B light, because in that fit the inner part of the region included the very blue annulus, or “hump,” at $r \approx 120''$. If extrapolated to the center, the blue surface brightness of the smooth “old disk” is about 20.85 mag arcsec $^{-2}$.

Azimuthal profiles of the “old disk” are presented in Figure 4. At inner radii the bar and at larger radii the loci of the arms dominate these plots, with “amplitudes” (trough to peak) of a factor of ~ 2 in intensity at nearly all radii. These surprisingly larger amplitudes must, however, be viewed with caution; they are substantially reduced if a higher inclination is assumed. For example, if

an inclination of 46° is assumed (obtained by Danvers [1942] from fits of logarithmic spirals to the inner spiral features, and about the highest tenable choice), the amplitudes of the bar and arms are reduced by about a factor of 2. However, it is important to emphasize that the azimuthal structure in these plots, corresponding to the bar and spiral arms in the galaxy, cannot be eliminated by any choice of position angle and inclination for the galaxy, nor by more stringent color selection in the algorithm illustrated in Figure 2. Rather, the azimuthal variations displayed in Figure 4 are produced from azimuthal variations in the smooth, relatively red inter-arm regions of this galaxy. This is exactly the same behavior as was discussed in detail by Schweizer (1976) for M51 and also noted by him for the other five galaxies in his study, corroborated by Jensen (1977) by infrared surface photometry of M51, M100, and M101, and also noted by Strom, Jensen, and Strom (1976) for two “smooth spirals” in which star formation in the arms is apparently absent. These authors have all suggested that this characteristic spiral-shaped variation in the surface brightness of the old population of these late spirals may simply be a density wave propagating through these old stars.

Finally, it is worth emphasizing that our technique very likely *underestimates* the amplitude of the azimuthal

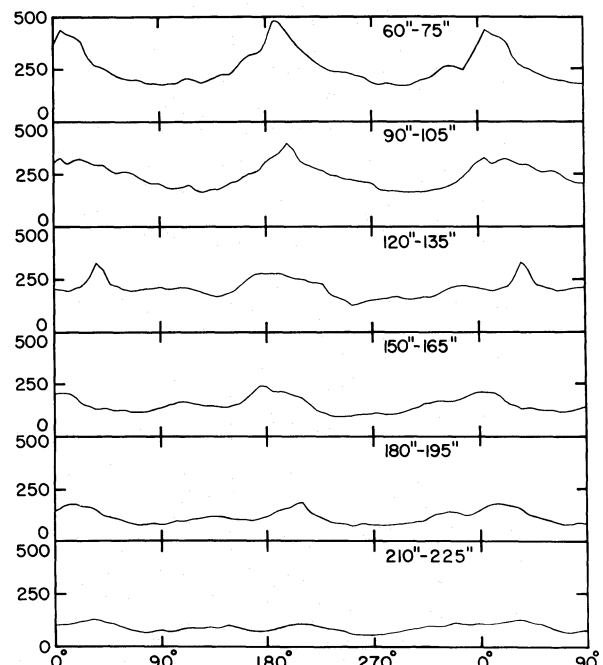


FIG. 4.—Azimuthal V profiles of the disk component at various radii in the plane of the galaxy, assuming an inclination of 24°. The ordinate of each profile is the linear flux scale used in this series of papers: One flux unit corresponds to $\mu = 27.5$ mag arcsec $^{-2}$. The abscissa is angular distance in the plane of the galaxy measured counterclockwise from the position angle of the major axis, taken to be 45° (NE) in the plane of the sky. The surprisingly large amplitudes shown in this figure must be viewed with caution; they are substantially reduced if a higher inclination is assumed.

variation in the old disk, since because of the ubiquity of blue regions in the vicinity of the peaks of the arms, we must interpolate across the peaks of these regions, which are likely to be the loci of the peak amplitude of the old disk as well. We have investigated several techniques to obtain a direct estimate of the contribution of the old disk in regions where it is masked by the presence of bright young associations. One such technique is to fit a low-order azimuthal Fourier series to the data at each radius; another is to assume an extinction at each pixel and use the U , B , and V fluxes of the pixel, "corrected" for this extinction, and the known disk color, to solve directly for the "disk" and "cluster" contributions to the pixel. Both of these techniques yield estimates for the "old disk" in the vicinity of the inner arms 10–20% higher than our interpolation technique. Fortunately, an error of this size would make no significant difference in any result presented in this paper. The errors that propagate from an error of this magnitude into the colors of the bright associations in the arms, whose ages and extinction-corrected luminosities we are attempting to measure, are inconsequential, because these associations are so much brighter than the disk. We have verified this by detailed calculations for several of the brighter associations that lie along the inner arms. The relative contributions of the young and old components are illustrated in Figure 5, where the "old disk" luminosity we have derived is plotted along with the total U , B , and V fluxes as a

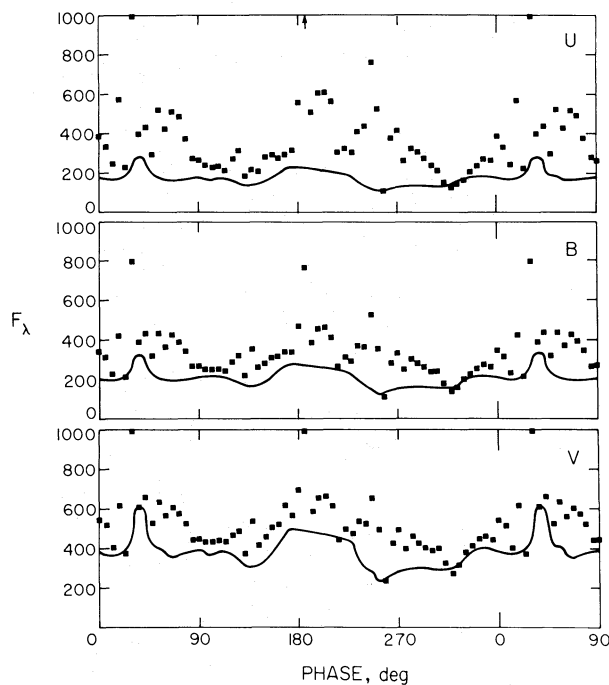


FIG. 5.—The U , B , and V azimuthal profiles in the annulus $120'' < r < 135''$. The "smooth disk" profiles are plotted as solid lines; the squares are the original data binned into $6''$ bins (in the plane of the galaxy). The scales of ordinates and abscissa are defined in Fig. 4. The anomalous bump at 30° phase is due to imperfect removal of one bright, anomalously red young stellar association in the arm.

function of azimuth in the radial bin $120'' \leq r \leq 135''$. As Figure 5 illustrates, the young blue stellar component often dominates the spiral arms. In fact, this dominance is more dramatic than Figure 5 shows, because of the large number of pixels in each bin in Figure 5.

IV. THE YOUNG STELLAR COMPONENT

In this section we describe the procedures by which the contribution of the young population to the light of each pixel has been obtained, and present results in the form of maps of the luminosity, "age," and "mass" distributions of the young population, and a map of the extinction we have calculated to the young component in each pixel. As we discussed in the Introduction, we assume that the integrated young light from a single pixel, if any such light is present, is comprised of a group of stars which formed approximately simultaneously and with a power-law IMF similar to the Salpeter IMF over the mass range we can observe ($> 3 M_\odot$). Therefore, each stellar group will evolve with time following a known track in the $(U - B, B - V)$ color-color plane, and so the ages of the groups may be derived.

In order to calculate the contribution to each pixel from the young component, it is necessary to subtract the contribution from the old disk and to correct for extinction. In the absence of extinction this would be a simple matter: once the old disk surface brightness F_λ^D has been determined (via § III) for each color $\lambda = U, B, V, R$, then the "cluster" component would be

$$F_\lambda^C = F_\lambda - F_\lambda^D, \quad (10)$$

where F_λ^D is known and F_λ is the observed intensity of the pixel. In the absence of extinction we would expect (with our assumptions) that the color of the young light of the pixel, after subtraction of the disk, would fall directly on the cluster evolution track. In practice, colors of pixels in the arms after simple subtraction of the underlying disk component usually fall to the right of the cluster evolution line in the $(U - B, B - V)$ plane, suggesting the existence of typically $\frac{1}{2}$ –2 mag of extinction (in B) to the young component.

If the light from the "cluster" in a pixel suffers extinction, then the contribution from the disk is likely to suffer extinction as well. Because the geometrical relationship between the "cluster," disk, and extinguishing medium is unknown, this problem cannot be solved uniquely. The simplest way to calculate the extinction is to subtract the disk light from the pixel and then calculate the extinction necessary to transform the color of the residual light to the cluster evolution track. In order to provide the reader with some general insight into our technique, this procedure is illustrated graphically in Figure 6a, where the light of a "typical" arm pixel, indicated by an open circle, has subtracted from it the (known) disk contribution, of color D, leaving a residual whose color is indicated by the filled circle. The remaining distance between this point and the cluster evolution track is taken to be due to extinction; this extinction is found by projecting back along the reddening vector (given by the

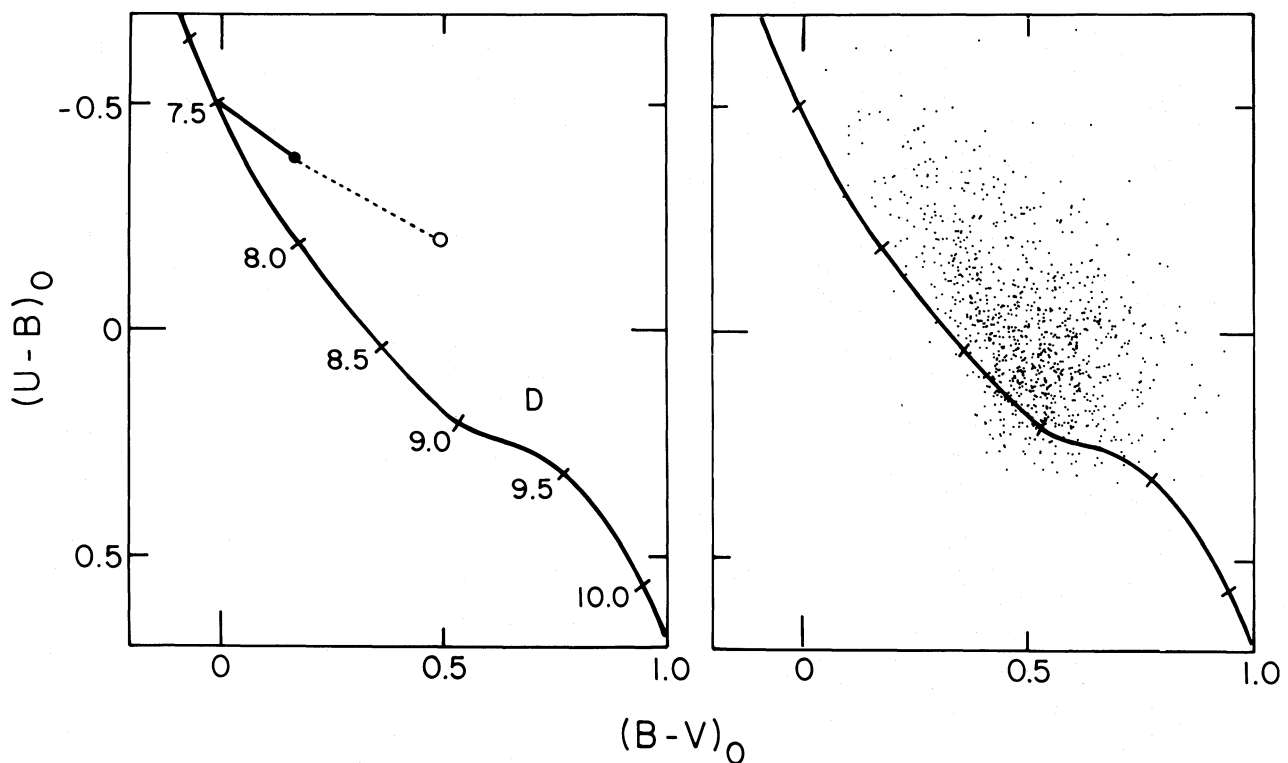


FIG. 6.—The left panel (6a) is a plot in the (color, color) plane of the cluster evolution track using the IMF of eq. (6). The open circle plotted is intended to represent a “typical” pixel in a bright blue patch in one of the arms in M83. Subtraction of our estimate of the disk light contribution to this pixel (whose color is indicated as a “D” on the plot) moves the point bluewards, as shown by the dotted line and the filled circle. The remaining distance between the point and the cluster evolution track is accounted for by extinction, illustrated by the solid line. It can be seen that this procedure produces an estimate for the age of the cluster light in the pixel. The right panel (6b) is a random sample of data from the annulus $100'' \leq r \leq 125''$ along with the same cluster evolution track plotted in 6a.

Whitford law). In Figure 6b the colors of a random sample of pixels in the annulus $120'' < r < 135''$ are plotted. The points whose colors lie near D in Figure 6a are almost invariably in the interarm. The arm data, for which generally $(U - B)_0 < 0.0$, can, with uniform success, be interpreted by the simple scheme illustrated in Figure 6a.

However, the arm regions in maps made by subtracting the “old disk” derived in § III from the total light are rather smooth at least on scales of a few pixels, implying that extinction (and star formation itself) is correlated over distances of at least a few pixels (~ 100 pc). If so, then applying the extinction derived for a pixel only to the cluster light in the pixel seems an unsatisfactory approximation. On the assumption that the extinction is at least roughly confined to the central plane of the galaxy, the extinction derived for a pixel should be applied to half the disk light as well.

To clarify this point, the expected geometrical relationship between the old disk, the obscuring layer, and the young “clusters” is illustrated in Figure 7. In this picture, where the dust is located in the midplane of the old population and young clusters occur somewhere within

the dust layer, the total flux from a pixel may be written as

$$F = F_\lambda^D(\frac{1}{2} + \frac{1}{2}10^{-0.4A_\lambda}) + F_\lambda^C(\text{age})10^{-0.4A_\lambda}, \quad (11)$$

where F_λ^D and $F_\lambda^C(\text{age})$ are the unobscured surface brightnesses of the disk and cluster in the pixel, A_λ is the

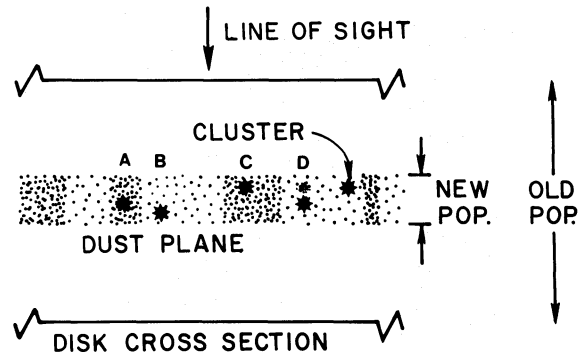


FIG. 7.—This is a schematic illustration of some of the possible geometries relating young clusters, dust clouds, and the young and old populations in the disk of M83. The specific examples of clusters, labeled A, B, C, and D in the diagram, are discussed in the text.

total extinction in the pixel, and ξ ($0 \leq \xi \leq 1$) is the fractional depth of the cluster within the dust layer. E.g., the cluster might be on the observer's side of the dust (C) and suffer little or no extinction. The simple (to calculate) case we just discussed and illustrated in Figure 6a, where the extinction applies only to the cluster component, is shown in Figure 7 as cluster D. However, this simple technique was *not* used to derive the cluster luminosity, age, and extinction maps we present in this paper. Because the data show that the extinction (and cluster component) is correlated over areas of at least a few pixels, we adopted the following two-step algorithm which applies the extinction to half the disk light to calculate the maps of cluster luminosity, age, and extinction we present in this paper:

1) We first employ the set of three equations (11) for U, B, V , and use $\xi = \frac{1}{2}$. We have three observed quantities (F_U, F_B, F_V) and three unknowns (A_B , "cluster" age, and "cluster" brightness F_B^C). The adoption of the Whitford law provides the other A_λ 's and the adopted cluster track provides the other F_λ^C 's. When there is a physically meaningful solution to these equations, it does not prove that $\xi = \frac{1}{2}$, but rather only that the assumption $\xi = \frac{1}{2}$ gives a consistent solution.

2) We have found that when procedure (1) fails to find a solution, it is caused by A_λ being simultaneously too small to adequately suppress the old disk light and yet too large to permit the cluster light to give the observed blue color (cluster C of Fig. 7). We therefore obtain a solution by assuming that A_λ is in fact large enough to completely suppress half of the disk light, but that this particular "cluster" is experiencing much less extinction, i.e., $\xi \ll 1$. For these pixels we solve for the three parameters $A_\lambda^C = \xi A_\lambda$, "cluster" age, and "cluster" brightness F_B^C in the expression

$$F_\lambda = \frac{1}{2}F_\lambda^D + F_\lambda^C(\text{age})10^{-0.4A_\lambda^C}. \quad (12)$$

We have applied this algorithm to each pixel in the image to produce maps of the unextincted blue "cluster" light, the log of the age of the "cluster," and the blue extinction to the cluster (either $\frac{1}{2}A_B$ from procedure [1] or A_B^C from procedure [2]). In addition, from the "cluster" luminosity and age we compute $\log M$, the logarithm of the "mass" of the "cluster." Figure 8 (Plate 13) displays the results. The cluster mass for real clusters is expected to be dominated by the unobservable behavior of the IMF at the low-mass end; consequently our $\log M$ should be regarded only as an indicator of the way the total mass of the "clusters" varies, assuming a common power-law IMF for all "clusters" in this galaxy. However, for illustrative purposes the "cluster mass" map can be normalized to $\log [\text{solar masses per pc}^2]$ for the IMF we used (defined by eq. [6]) by subtracting 0.2 from the logarithms in the map.

To reduce the noise, all pixels in Figure 8 whose flux in any passband fell within 20% of the old disk flux were suppressed. There still remains some mottled noise near the periphery of the region studied. The region inside $R = 15''$ was suppressed since our calibration was uncertain in this region. The long features in the lower right and

at the top are artifacts created by scratches on one of the plates. For the purpose of convenient intercomparison, the two lower panels of Figure 8 show the $H\alpha$ flux displayed in R magnitudes⁴ and the $U - B$ color. The latter clearly illustrates how the population separation algorithm pinpoints regions rich in ultraviolet. One of the striking features of the $H\alpha$ image is that in some areas it looks very different from the other images. This is because the $H\alpha$ data emphasize those regions dominated by the most massive stars (O6 and earlier), i.e., those which produce the largest ionizing fluxes in comparison with their U, B, V fluxes. The $U - B$ and other pictures emphasize those stars relatively less. In the inner arms on the east and west sides the $H\alpha$ and other images are similar. In contrast, in the outer arms there are significant differences. This suggests that there are variations in the high-mass end of the IMF in this galaxy.

V. INTERPRETATION OF RESULTS

In this section, we explore some of the characteristics of the "cluster" age, luminosity, and "mass" distributions we have derived. Among the more remarkable of these characteristics are the existence of recently formed stars in essentially every pixel in the arms, the very large number of young massive stars, and the chaotic distribution of the ages of the associations. In much of our analysis of the data, we employ as a standard for comparison the Salpeter-like IMF defined previously. However, there are a variety of indications in our data that such a power-law IMF is a thoroughly inappropriate approximation to the star-formation processes that we are observing in the inner arms of M83. In the following discussion we point out some of these indications as they arise, and then attempt a coherent discussion of the IMF at the end of the section.

a) An Interesting Region

It is important to investigate to what extent our maps are influenced by statistical noise. In order to improve our feel for our data, to be sure that the features in the maps in Figure 8 are not substantially influenced by statistical noise, and to study the smaller-scale structure of M83, we have studied several especially interesting regions of M83 in detail, often on a point-by-point basis. We have assembled 12 different maps of one such region into Figure 9 (Plate 14). We selected this particular region for presentation because it contains good examples of what we interpret as young "clusters" of several ages, some with $H\alpha$ emission and others without, and also because it contains a portion of a dust lane and of the old disk interior to the dust lane. Another reason we selected this region for presentation is because it contains one of the best examples in the galaxy of a "cluster" (labeled "B" in Fig. 9) that is both older and brighter (in the B passband) than several other clusters around it.

Data from the labeled locations in Figure 9 are plotted in the (color, color) plane in Figure 10. The colors of two

⁴ $H\alpha$ in R magnitudes means the intensity of $H\alpha$ as measured by using a standard R passband photometer.

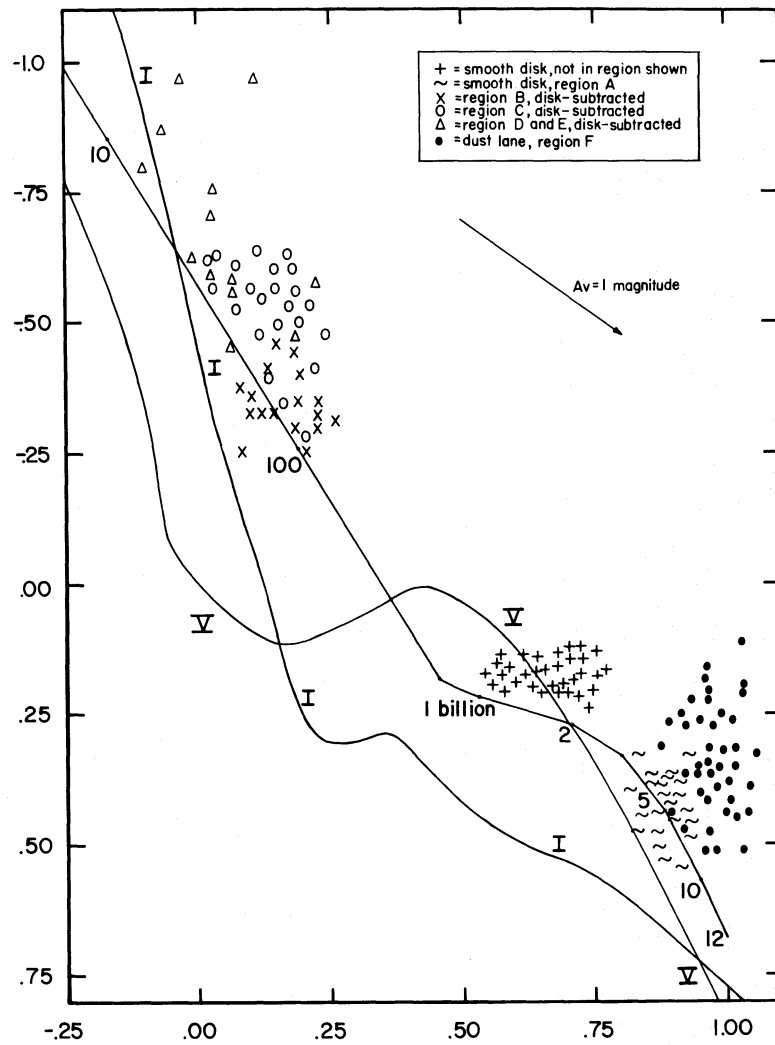


FIG. 10.—A standard color-color diagram. The tracks labeled "I" and "V" are supergiant and main-sequence stellar tracks from Johnson (1966). The other track shown is a cluster evolution track we have calculated; the numbers along it are ages in 10^6 yr toward the top and 10^9 yr toward the bottom. The symbols plotted represent colors of individual pixels in various regions of M83 as noted in the key.

separate regions of "old disk" are shown in Figure 10. The "old disk" region A of Figure 9, although adjacent to the clusters labeled B, C, D, and E, corresponds to a smaller galactocentric radius. Data from an "old disk" region at roughly the same galactocentric radius as the clusters is also shown in Figure 10 (as +'s), since this is approximately the color of the light that was subtracted from the clusters B-D. This region is located just interior to the dust lane, like region A, but 55" (~ 1 kpc) below the bottom of the area shown in Figure 9. From our consideration of data such as illustrated in Figure 9 and Figure 10 we conclude that except for dust patches, we can successfully interpret the intensity and colors of the galaxy in the terms of our simple picture involving disk light, "cluster" light, and extinction, and that our maps are not strongly affected by systematic errors, such as intensity-dependent errors, in our deconvolution procedure.

b) The Radial Color Gradient in the Old Disk

The difference in color between the two disk regions shown in Figure 10 is illustrative of the substantial color gradient in the inner part of the "old disk" we found in § III. There are at least three possible causes for the radial color gradient in the old disk. Unfortunately, our broad-band *UBV* photometry provides insufficient information to distinguish among them. The color gradient is probably caused at least in part by a systematic variation in the star-formation history as a function of radius, as suggested by the correspondence between the "old disk" colors in Figure 10 and the cluster evolution track also plotted there. However, since there is an oxygen abundance gradient in the gas in the inner part of M83 (Dufour *et al.* 1980), it is likely that there is also a gradient in the mean metallicity of the intermediate-age stars that contribute most of the light, and this will contribute to the

observed color gradient as well. Furthermore, since the dust reddening line and the cluster evolution track for ages greater than two billion years are nearly parallel in the (color, color) plane, a smooth distribution of dust concentrated toward the central region of the galaxy would also produce the observed color gradient.

Apparently, such old disk color gradients are not typical in spirals. Schweizer (1976) found a similar old disk color gradient in only one (M81) of the six spirals he studied. Of the other five, it is perhaps most remarkable that he found no such gradient in M100 (NGC 4321), since it is a near morphological twin to M83. In addition, Hoessel and Melnick (1980) report the absence of an old disk color gradient in M31. Unless the old disk color gradient in M83 is due to dust, which would be perverse, especially since the distribution of such dust would have to be anticorrelated with the distribution of H I, the color gradient we observe has the potential of furnishing valuable evidence concerning the star formation history and chemical evolution of the disk of M83, should it ever be studied with a spectrophotometric system such as that of Boroson (1980) capable of distinguishing among the effects of stellar age, metallicity, and dust extinction.

c) Colors of Dust Lanes

We have also plotted in Figure 10 data from the center of the dust lane shown in Figure 9. These data occupy a peculiar locus in the (color, color) plane. We obtain such colors not just from this dust lane but from wherever in the galaxy we plot the colors of dark, apparently optically thick clouds. As can be seen from inspection of Figure 10, we can obtain formal deconvolutions of such data from our model by invoking very large extinctions and moderately old ($\sim 10^8$ yr) "clusters." Such "solutions" seem contrived, however, since such dust patches are often found in the interarms, without any evidence for the presence of any stellar population other than what is present in adjoining old disk regions. We conclude that such data cannot be correctly interpreted within the constraints of the simple ideas which we have used with success throughout most of the galaxy.

It seems likely that these data display the effects of differing optical depth of the dust features in the different passbands, with some evidence for wavelength-dependent scattering of light from stars in front of the dust features. A recent investigation of the dust features of the four spiral galaxies M74, M51, M101, and NGC 7793 by D. Elmegreen (1980a) has been of some use to us in our analysis of this problem. She employed *UBVRI* surface photometry and a detailed, multiparameter treatment of the radiative transfer in the region of the galaxy with the cloud. None of Elmegreen's models display the exact behavior of the dust patches we have measured in M83; in particular, none get bluer in $U - B$ as much of our data and some of her data do. However, her models produce a wide range of colors despite the limitations of her parameter space. It seems certain that an appropriate model (perhaps with a wavelength-dependent dust albedo)

could be found to match our data. Further consideration of these problems are, however, beyond the scope of this paper.

d) The Gigantic Star-Formation Rate

Perhaps the most remarkable feature of the star formation in M83 is the enormous number of newly formed hot luminous stars in the large clumps strung along the inner arms. (We follow Wray and de Vaucouleurs 1980 in labeling such clumps "superassociations.") The star formation in these superassociations is large compared with both the solar neighborhood and rates predicted by simple models of spiral galaxy evolution. For example, in the inner 150" (2.74 kpc), a region encompassing the inner arms but not the less organized features farther out, the total Lyman continuum flux as deduced from the $H\alpha$ flux corrected for extinction amounts to 3.6×10^{42} ergs s $^{-1}$, equivalent to 2500 O5 stars or 3.0×10^5 BO V stars. As gigantic as these numbers seem in comparison with well-studied complexes of star formation in the solar neighborhood, they are evidently not unusual in late spirals. The superassociations along the inner arms of M83 are no different than the equally gigantic associations in the arms of M101, such as NGC 5461 whose Lyman continuum flux was first estimated by Searle (1971) from spectrophotometry of $H\alpha$ and of $H\beta$ and later by Israel, Goss, and Allen (1975) from Westerbork synthesis observations at 6 cm, 21 cm, and 49 cm. By comparison, the total Lyman continuum flux in the inner region ($r < 6$ kpc) of the Milky Way amounts to about 3.7×10^{42} ergs s $^{-1}$, 2570 O5 stars, or 3.1×10^5 BO V stars (from data of Smith, Biermann, and Mezger 1977 and Mezger 1978). In both galaxies there exists a nearly ring-shaped zone where the rate of formation of massive stars is large, both absolutely and in comparison with regions farther from the center. Both galaxies have a region of active star formation surrounding the nucleus, as well. This is obvious in the case of M83; for the Milky Way, the evidence comes from infrared and radio observations (Oort 1977). Also, it is perhaps worth mentioning that the Milky Way may have a bar in its inner region, as has been repeatedly suggested by de Vaucouleurs (1964, 1970). The possible driving of the 3 kpc arm by such a bar has been discussed by several investigators (see, e.g., Kerr 1967; Sanders 1977; Roberts 1979a). Furthermore, the case for the existence of a bar in our Galaxy appears to have been considerably strengthened by the recent re-interpretation of the dynamics of the gas in the Galaxy's inner regions by Liszt and Burton (1980) in terms of stationary or quasi-stationary tilted elliptical streamlines. These facts suggest that M83 and our Galaxy may be quite similar.

In order to compare the estimates of the star-formation rate we deduce from our observations with those predicted by simple models, we have collected our two empirical estimates and three simple theoretical estimates of this quantity, each computed for 12 annular rings, into Table 1. The various results for each ring appear in the five columns labeled $B [M_{\odot} pc^{-2}(10^9 yr)^{-1}]$, which is the

M83: STAR FORMATION IN ANNULAR RINGS

Radius	Total H _a Emission arcseconds kpc	H _a total Star Formation	B _{Ha}	UBV Total Star Formation	B _{UBV}	Σ [total]	Σ _{gas}	B _{mass}	B _{gas}	B _Z	P _Z	
	arcseconds photons s ⁻¹	M _O Gyr ⁻¹	M _O pc ⁻² Gyr ⁻¹	M _O Gyr ⁻¹	M _O pc ⁻² Gyr ⁻¹	M _O pc ⁻²	M _O pc ⁻²	M _O pc ⁻² Gyr ⁻¹	M _O pc ⁻² Gyr ⁻¹	M _O pc ⁻² Gyr ⁻¹	yield	
0- 15"	0.00-0.27			3.8 × 10 ⁷	164	2000 (5520)	24	0.036	154	8.2	2.3	
15- 30	1.07 × 10 ⁶	7.1 × 10 ⁷	101	16.6	237	1820 (2240)	24	.050	140	8.0	3.2	
0.27-0.55											.012	
30- 45	0.75	4.9	42	16.6	142	1620 (1140)	23	.100	125	7.5	6.2	
0.55-0.82											.024	
45- 60	0.14	0.90	5.5	23.1	141	1450 (1480)	22	.125	112	7.1	7.4	
0.82-1.09											.030	
60- 75	0.30	2.0	9.4	15.0	71	1290	21	.115	99	6.7	6.5	
1.09-1.36											.028	
75- 90	0.34	2.3	8.8	14.6	57	1150	20	.106	88	6.2	5.7	
1.36-1.64											.026	
90- 105	0.51	3.4	11.2	21.7	72	1020	19	.096	78	5.8	4.9	
1.64-1.91											.024	
105- 120	1.85	12.2	35	45.0	128	910	19	.086	70	5.7	4.4	
1.91-2.18											.022	
120- 135	1.36	9.0	23	38.7	98	830	18	.075	64	5.3	3.6	
2.18-2.46											.020	
135- 150	0.82	5.4	12.2	34.7	78	740	18	.065	57	5.1	3.2	
2.46-2.73											.017	
150- 165	0.73	4.8	9.8	26.4	54	661	17	.059	51	4.8	2.7	
2.73-3.00											.016	
165- 180	0.62	4.1	7.7	20.5	38	589	16	.058	45	4.4	2.5	
3.00-3.27											.016	
(1)	(2)	(3)	(4)	(5)	(6)	(7) disk only (disk + spheroid)	(8)	(9)	(10)	(11)	(12)	(13)

Explanation of Quantities in Table 1

- 1) Inner and outer radii of annulus in arcsec and kpc, using 3.75 Mpc distance (de Vaucouleurs 1979).
- 2) Total H α emission from observed H α (Fig. 8), corrected for extinction using extinction map in Fig. 8.
- 3) Total rate of star formation in annulus derived from H α emission, assuming IMF of eq. (6), and the following total Lyman continuum flux per unit mass for this IMF:

$$\frac{\int_{\text{time}} \text{Ly-continuum photons}}{(\text{M}_{\text{cluster}}/\text{M}_\odot)} = 8.58 \times 10^{60},$$

which was derived using the O star data tabulated by Panagia (1973) and O star lifetimes ($4-8 \times 10^6$ yr) tabulated by Davis (1979), the sources of which were listed earlier in this paper. Our calculation makes no completeness corrections but simply assumes that all Lyman continuum photons produce H α which, allowing only for the extinction we can measure, we count. It is thus a *lower limit* on the rate of production of massive stars expressed (quaintly) in terms of masses of hypothetical star clusters with the IMF defined in eq. (6). Talbot (1980) used the same data H α to derive a star-formation rate for M83. He used a cruder extinction correction; our correction makes no significant difference except to increase the derived flux somewhat in the $105''-135''$ bins. However, the star formation rate ($B_{\text{H}\alpha}$) we derive here is significantly smaller than that derived by Talbot because the number of Lyman continuum photons per solar mass of cluster material (8.58×10^{60}) we have derived is some 3 times larger than the number used by Talbot, which was derived by Smith, Biermann, and Mezger (1977) and Mezger (1978) for use with galactic radio data.

- 4) Rate of star formation per unit area derived from H α .
- 5) Total rate of star formation in annulus derived from UBV maps using results of § III and § IV, presented as maps in Fig. 8, converted to a rate by counting only cluster mass younger than 40×10^6 yr and dividing by 40×10^6 yr.
- 6) Rate of star formation per unit area derived from UBV .
- 7) Total mass per unit area in disk component (and total of disk plus spheroid in parenthesis), from a rotation curve we derived from velocity field data (generously provided to us in advance of publication by Charles Peterson) by a least-squares fit to a two-component mass model constrained to fit the light distribution.

$$\text{spheroid: } \frac{M}{L} = 2, \mu_B = 20.497 + 8.327 \left[\left(\frac{r}{18.37} \right)^{1/4} - 1 \right],$$

$$\text{disk: } \frac{M}{L} = 7.11, \mu_B = 20.85 + 1.822 \left(\frac{r}{237''} \right).$$

- 8) Current surface density of gas as deduced by Talbot (1980) from the H I map of Rogstad, Lockhart, and Wright (1974) and the CO data of Combes *et al.* (1978).

- 9) Mass fraction of heavy elements in the gas inferred from spectroscopic observations of six H II regions in M83 by Dutour *et al.* (1980).

- 10) Mean rate of formation of stars over assumed lifetime of 13×10^9 yr:

$$B_{\text{mass}} = \bar{B} = \frac{\sum_{\text{disk}}}{T}.$$

- 11) Present rate of formation of stars per unit area to deplete the gas to its present level if (a) no radial gas flows; (b) no infall from outside system; (c) star formation rate per unit mass of gas, $\nu = B \sum_{\text{gas}}$, is constant with time (but not necessarily with position r); i.e., the exponential model:

$$B_{\text{gas}} = \frac{\sum_{\text{gas}}}{T} \ln \left(\frac{\sum_{\text{disk}}}{\sum_{\text{gas}}} \right).$$

- 12) Current rate of star formation in a model constrained to produce the observed heavy element abundance with an assumed yield of heavy elements per generation $p = 0.0285$ (calculated for our IMF, eq. [6], from the yields per star given by Arnett 1978), and assuming a star-formation rate proportional to current gas density.

- 13) Yield of heavy elements per generation necessary to produce the observed B_{gas} with our IMF (eq. [6]) and the exponential star formation model (eq. [15]).

rate of formation of stars per unit area, estimated in the following five ways:

1. $B_{H\alpha}$ is the rate obtained from the $H\alpha$ map in Figure 8, after correcting for extinction pixel by pixel, using the extinction map in Figure 8, assuming the IMF defined in the Introduction (which was truncated at $60 M_\odot$). A fuller definition of our derivation of this quantity appears in the notes to the table.

2. B_{UBV} is the rate obtained from the "cluster mass" map in Figure 8, which was derived from the "cluster luminosity" and "cluster age" maps in Figure 8, again assuming the same IMF. The data here are derived from integrals of the appropriate regions in Figure 8 for pixels with ages less than 40 million yr. That is, we here deduce a star formation rate by counting all clusters brighter than 20% of the disk whose derived ages are less than 40 million yr, and by assuming these clusters have the Salpeter-like IMF given in the Introduction:

$$B_{UBV} = \frac{\sum_{\text{annulus}} (\text{mass of "cluster" in pixel from Fig. 8})}{(\text{area of annulus}) \times (40 \text{ million yr})} \quad (13)$$

3. B_{mass} is the mean past rate of star formation in order to turn all of the mass in an annulus into stars over the lifetime of the galaxy:

$$B_{\text{mass}} = \bar{B} = \frac{\sum_{\text{total}}}{T}, \quad (14)$$

where \sum_{total} is the total mass surface density of the galaxy, derived from the rotation curve, and where for T , the age of the galaxy, we use 13×10^9 yr.

4. B_{gas} is the present rate of star formation predicted by the simple model where the galaxy is assumed to begin as a disk of gas, and star formation occurs at a rate proportional to the current gas density:

$$\frac{d \sum_{\text{gas}}}{dt} = -B_{\text{gas}}(t) = -v \sum_{\text{gas}},$$

where the proportionality factor v is constant with time, but not necessarily with radius. Then the present rate is

$$B_{\text{gas}} = \frac{\sum_{\text{gas}}}{T} \ln \left(\frac{\sum_{\text{total}}}{\sum_{\text{gas}}} \right). \quad (15)$$

5. B_Z is the present star formation rate required to have produced the observed heavy element abundance in the gas, assuming a yield of heavy elements per star of a given mass and neglecting gas flows:

$$B_Z = \frac{Z \sum_{\text{gas}}}{pT}. \quad (16)$$

For p , the fractional yield (by mass) of heavy elements per generation of stars, we use 0.0285 which we have derived for our IMF (eq. [6]) from the supernova yield calculations tabulated by Arnett (1978). Rather than assume a yield and compute B_Z from it, it is perhaps more useful to estimate the mean yield necessary to produce the ob-

served gas heavy element abundance in each annulus directly via

$$p = \frac{Z}{\ln (\sum_{\text{total}} / \sum_{\text{gas}})}. \quad (17)$$

This quantity is tabulated in column (13).

The remaining columns of Table 1 were calculated in order to derive the five estimates of B . Their definitions and derivations are listed in the notes to the table. The essential fact that should be understood in studying the table is that, if the simple model with a constant, solar neighborhood-like IMF and no gas flows were valid, all B 's (except B_{mass}) in a given annulus would be identical.

The following conclusions can be drawn based on the quantities tabulated in Table 1:

1. The star-formation rate we estimate from the $H\alpha$ flux falls below that estimated from the UBV by a factor of 3–4 in the rings with the most vigorous star formation, and by factors of 8–25 in the other rings. Some of this is undoubtedly due to preferential obscuration of the youngest stars. However, we are comparing these rates to one another using the Salpeter function, in whose derivation the same selection would be expected to apply. In fact, however, the IMF for $M > 10 M_\odot$ is not well determined either for the solar neighborhood or anywhere else. In the solar neighborhood, the evidence appears to favor a power-law IMF with the power-law exponent ~ 2.0 for high masses (Lequeux 1979). This would produce a ratio of O4–O6 to O7–B3 stars different than the ratio given by the Salpeter exponent (1.35) by a factor of ~ 0.6 , which is insufficient to explain the discrepancy in Table 1. It is therefore difficult to escape the conclusion that the distribution of effective temperatures of newly formed massive stars is different at different sites in M83 and substantially different from this distribution in the solar neighborhood. This observation could be the consequence of an initial mass function in M83 that favors the production of $8\text{--}25 M_\odot$ stars over those more massive, as compared with the solar neighborhood. In fact, the high metal abundance in the gas of this inner region of M83, typically $\sim 4 Z_\odot$, might lead to such a change in the IMF, due to enhanced dust opacity opposing the infall of the latter stages of protostellar collapse (Kahn 1974; Shields and Tinsley 1976). On the other hand, it is possible that the massive stars we are observing in M83 suffer substantially greater blanketing of the Lyman continuum than those of the same mass in the solar neighborhood, due to their higher metal abundance. It is even possible that these stars are substantially *colder* (at a given mass) than those in the stellar evolution calculations we used, because of the much greater opacity in the envelopes and atmospheres of those high- Z stars. (The interior opacities, being due to electron scattering, would not be significantly different.) This opacity effect has been illustrated for $Z = 0.02$ and $Z = 0.04$ by Stothers and Chin (1977).

2. The star-formation rates we estimate from the $H\alpha$, and particularly from the UBV colors, greatly exceed (by factors of 10–20 for B_{UBV}) the rate we derive from the

present gas density in a model where the star formation proceeds at a rate proportional to the gas density (exponential decay) using the solar neighborhood IMF. The rate estimated from the UBV colors (dominated by B stars) equals or exceeds the mean past rate (B_{mass}) in most of the annuli. Furthermore, the inferred B_{UBV} is sufficient to consume all of the existing interstellar gas in from 100 to 300 million yr, depending on the annulus. If we are to maintain that star formation in M83 is in rough equilibrium, that is, that the galaxy will continue to have a star-formation rate (and morphology) roughly similar to its rate and morphology as present, we are forced to abandon the simple idea of a "universal" IMF. The sites of O and B star formation we observe in M83 are making low-mass stars *at least 10 times less efficiently* than the solar neighborhood IMF predicts. Furthermore, this disparity between the observed rate of formation of massive stars and the total rate of mass consumption inferred from the gas density (and dominated by low-mass stars) is a strong function of radius, peaking in the 105° – 135° region. It seems natural, therefore, to speculate that the production of stars of a solar mass or less may be completely disconnected from the production of high-mass stars. If so, then the conversion of gas into long-lived, low-mass stars and the conversion of gas into heavy elements via nucleosynthesis in massive stars are consequences of different processes, occurring in different sites in the galaxy, most probably at independent rates. This result has also been obtained for M83 and our Galaxy from somewhat different considerations by Talbot (1980). The same discrepancy between the available gas mass and the mass of star clusters predicted by extrapolation from the number of high-mass stars using the Salpeter function is also present in the large H II complexes in M101.

It follows that existing models of galaxy evolution such as those of Larson (1976), in which the nucleosynthesis rate and total star-formation rate are proportional, are unlikely to adequately represent the evolution of real galaxies. This view is strengthened by the evidence (Elias 1978a, b; Elmegreen 1980b; Lada, Blitz, and Elmegreen 1979; Eggen 1976, 1977) that in nearby regions of our Galaxy sites of low-mass and high-mass star formation are different. Unfortunately, the direct identification of sites of low-mass star formation in a galaxy such as M83 is a very formidable observational problem, well beyond what is possible with data such as ours. It perhaps should be added that with the steadily mounting evidence that the total mass distribution of galaxies such as M83 matches the distributions neither of the gas nor of any known luminous component (Faber and Gallagher 1979), the prospect for anything like satisfactory theoretical understanding of the structure and evolution of spiral galaxies any time soon seems dismal indeed.

3. The present rate of nucleosynthesis is apparently much more than adequate to account for the gas heavy-element abundance. The yields necessary to produce the existing gas heavy-element abundance in an exponential model, tabulated in column (13), are in fact in good agreement with the yield $p = 0.0285$ we have calculated

for our IMF from Arnett's (1978) tables. However, we have just argued that the ratio of the production of OB stars to low-mass stars must be as much as an order of magnitude greater than that predicted by our illustrative IMF. Therefore, the yield must be greater by almost the same factor. This apparent overproduction of heavy elements will be alleviated somewhat (perhaps by a factor of 2) if the IMF is deficient in the most massive stars. Resolution of the remaining discrepancy appears impossible with appeal to radial gas flows or infall, again unless we are observing M83 at a time of anomalously high star formation.

Assuming our estimate of the yield is crudely correct, if the arms are rigidly rotating waves, then the hypothesis suggested by Oort (1974) and investigated by Jensen, Strom, and Strom (1976) that density-wave driven star formation produces abundance *gradients* in galaxies becomes persuasive. However, the quantitative relations between the rate of star formation, rate of nucleosynthesis, and rate of ISM enrichment cannot be simple (Talbot 1980; Casse, Kunth, and Scalo 1979). In particular, if the present radial distribution of nucleosynthesis in M83 is representative of the past rate, then radial gas flows or infall of relatively pristine material must exist in order that the nucleosynthesis distribution be consistent with the current radial heavy-element distribution.

e) Ubiquity of Star Formation

Another remarkable feature of the star formation in M83, as shown by the maps displayed in Figure 8, is the ubiquity of star formation in the prominent inner arms. The $H\alpha$ luminosity map is dominated by a few associations (or "superassociations") lying like beads on a string along the inner spiral arms. However, in the "cluster" luminosity map, the regions *between* these associations are also filled in with young stars, albeit at a considerably lower average surface brightness. This distributed population of young stars in the arms also manifests itself as a color excess in the color maps published by TJD. Again, it is significant that the colors of *nearly every pixel* in the arms of M83 are bluer than the bluest pixels in the disk, even in the "reddening-free" color index Q .

It may be possible to explain this remarkable distribution of young starlight in terms of diffusion of young stars from their formation sites as they drift along the arm during the first few tens of million years after their births. A cluster velocity dispersion of 10 km s^{-1} leads to a size of 500 pc in only 50 million yr. This is rather close to the characteristic size we observe for blobs of light in the arms of age ~ 50 million yr. However, we are hesitant to accept the hypothesis that the appearance of the age map in Figure 8 is *dominated* by this diffusion process, as these numbers suggest. This is because the brighter star-formation regions, even those with ages comparable to 50 million yr such as the "cluster" labeled B in Figure 9, have sharp boundaries, as may best be seen in the $U - B$ and Q maps published by TJD. Furthermore, the whole locus of star formation defining the inner arms has sharp boundaries both on the inside and the outside. It seems possible, therefore, that to some extent the ubiquity of

pixels with young stars in them could be the result of a spatially widespread star-forming process.

If this conclusion is correct, it places an interesting constraint on the distribution of molecular clouds in M83, on the assumption that star formation occurs only in molecular clouds. The "constraint" is merely that, roughly speaking, there should be at least one molecular cloud per 27 pc resolution element in the arm region of M83. The total amount of mass involved would not be excessive. If the clouds were $\sim 10^4 M_{\odot}$ each, only $\sim 5 \times 10^8 M_{\odot}$ in molecular hydrogen would be required. However, the large space density of these clouds would be in striking contrast to the situation in the solar neighborhood. The scenario in which much of the star formation in the arms occurs as a direct consequence of disruption of a "standard cloud" by the galactic shock (Woodward 1976) has recently fallen out of fashion because this mechanism of star formation is not observed in the solar neighborhood (Lada, Blitz, and Elmegreen 1979). It is conceivable, however, that such a mechanism may in fact operate in the inner region of M83, where physical conditions of the ISM are greatly different than in the neighborhood of the Sun.

f) Young Star Age Distribution

Theoretical expectations.—It seems all but impossible to avoid the interpretation that the inner, symmetric arms of M83 are visible manifestations of density waves in the gas (and almost certainly in the stars as well), driven by the central bar, which is itself a wave with a pattern speed considerably slower than the mean orbital speed of the stars that comprise it. Such bars, stable and robust, usually develop in numerical models of stellar dynamical systems that have large angular momentum compared with their internal random motions (Miller and Smith 1979 and references therein). Such bars are not well understood theoretically, but simple self-consistent models consisting of a few stellar orbits have been constructed (Contopoulos 1979). The response of a disk of gas to a central slowly rotating barlike perturbation has been calculated by numerous investigators both for massless and self-gravitating gas (see Roberts 1979b for a recent review). Such models match well the H α velocity field of the barred spiral NGC 5383 (Huntley 1978; Peterson *et al.* 1978) and the shape of the dust lane in galaxies such as NGC 1300 (Roberts, Huntley, and van Albada 1979), making the plausible identification of the dust lane with the locus of the theoretically predicted shock in the gas. In addition, the steady-state distribution of gas obtained by stirring a self-gravitating, isothermal gas disk with a uniformly rotating stellar bar presented by Huntley (1979, 1980) bears an almost uncanny resemblance to the distribution of young stars in M83 we have mapped in Figure 8.

Within this picture of a bar-driven density wave in the gas, there are three models that have been suggested for the star formation in these density-wave arms. In the first of these, star formation is envisaged to occur as the consequence of the action of the shock on Spitzer's (1968) "standard" H I clouds (Roberts 1969; Shu *et al.* 1972).

Woodward's (1976) calculation has seemed to lend great plausibility to this model, but the mechanism has been criticized on the basis that no star formation observable in the solar neighborhood seems to be occurring as a consequence of this process. Instead, all known star formation occurs in association with giant molecular clouds that would not be significantly affected by an encounter with a galactic shock (Lada, Blitz, and Elmegreen 1979). A second mechanism invokes Parker's (1966) instability, triggered by the shock, to collect diffuse gas into giant molecular clouds in which star formation then proceeds spontaneously (Shu 1974; Mouschovias, Shu, and Woodward 1974). Blitz and Shu (1980) have recently argued that observations of nearby giant molecular clouds support the hypothesis that they were formed as a result of Parker instability.

Both of these mechanisms require the existence of a galactic shock associated with the gaseous density wave. However, if the interstellar medium in the inner part of M83 is dominated by 10^6 K gas, as is the case in the solar neighborhood, no shock will form, as was first pointed out by Scott, Jensen, and Roberts (1977; see also Shu 1978). On the other hand, it appears that the solar neighborhood may not be typical even of our own Galaxy (Heiles 1980). In view of the importance of this question, it is irritating that no direct kinematic evidence concerning the existence of galactic shocks in nearby spirals has yet been developed; even the H I observations of M81 by Rots (1975) can be fitted to a linear gas density-wave model, although nonlinear models are superior (Visser 1978). Tully's (1974) earlier study of M51 gave the same result. In addition to such kinematical studies, observations of the soft X-ray distribution in nearby spirals with the *Einstein* satellite would also clearly be of great relevance (van der Laan 1978).

A third possible mechanism, one that does not require the existence of the galactic shock, is star formation induced by cloud-cloud collisions. In this picture, clouds are envisaged as being relatively long-lived and distributed throughout the galaxy, forming a low-velocity-dispersion population of ballistic objects. If their collision mean-free path is short enough to treat the ensemble of clouds as a dissipative continuum, this model develops "shocks" like the galactic shock model (Talbot 1977; Shu 1978). In this case the "atoms" of the shocked gas are clouds rather than the atoms of the continuum fluid invoked in conventional gas dynamics models such as those of Roberts (1969) and Shu *et al.* (1972). The cloud-cloud collision-induced star formation would be largest where the cloud density is greatest, and would persist over several mean-free collision time scales. This model has recently been criticized by Blitz and Shu (1980), who argue that contrary to the previous interpretation of the distribution of molecular clouds in the inner regions of our Galaxy (Solomon and Sanders 1980; Scoville and Hersh 1979), such clouds cannot be sufficiently long-lived to persist across the interarm regions.

As we stated in the Introduction and previously (TJD), one of our principal motivations in undertaking this work was our interest in the "prediction" of the density-wave

theory of a wake of young stars aging gradually with increasing distance from the current locus of star formation. Ironically, however, despite early naive expectations to the contrary (cf. Schweizer 1976; Larson 1977; TJD), none of the possible star-forming mechanisms predict detectable color or age gradients in the vicinity of the arms. The case of the shocked cloud mechanism has now been investigated in detail by Bash (1979) and Yuan and Grosbol (1981), who find that the expected post-shock cloud velocity dispersion, the large radial component of the post-shock cloud orbits, and the expected spread in the formation time of stars in the wake of the shock ($\sim 10^7$ yr, Woodward 1976) will combine to completely smear the age distribution of the young stars. In the case of the Parker instability, differential delays of the order of 10^7 yr for the instability to develop can also be expected. The cloud-collision model predicts no age gradient in the vicinity of the arm to begin with.

An alternate, "stochastic" model of star formation in spiral galaxies has recently been proposed (Mueller and Arnett 1976; Gerola and Seiden 1978; Seiden and Gerola 1979), in which spiral structure in the young stars occurs as the result of the action of differential rotation on randomly situated chains of self-propagating star-forming events. We do not feel this model is applicable to the inner arms of M83 because the strong bilateral bar + arm symmetry is obviously related to the driving mechanism for the star formation in the inner arms: in the large scale, the star formation cannot be "stochastic." (See, however, Elmegreen 1979 for an attempt to combine some of the ideas of the stochastic model with the shocked cloud mechanism.) Also, it is possible that the stochastic model might apply to the more chaotic spirality of the young associations in the outer portions of M83.

The observations.—The "age" distribution of the OB associations in the arms of M83, as illustrated by the map in Figure 8, is totally chaotic. We have examined this distribution with great care for evidence of "drift," or aging relative to the inner edge of the spiral arms, conveniently defined by the dust lane. Except for an apparent tendency of the very youngest associations (identifiable both by the ages we measure from *UBV* and their H α flux) to concentrate on the inner edge of the arm close to the dust lane, a result most easily seen in the H α map, there is no evidence for any systematic change of age with position in the arm. This confirms the result of TJD, deduced from analysis of the original color maps. However, the existence in the interarm of smooth regions free of any star formation does place one constraint on the way star formation propagates through cloud complexes: whatever the mechanism is, it must cease to operate after a few tens of millions of years; otherwise, star formation would be observed continuing to operate in the smooth interarm region. What is evidently required to explain our observation is a star-formation mechanism that globally triggers formation of massive stars in an accurate two-armed spiral-shaped pattern, locally acts in a largely stochastic way over a distance scale of a few hundred parsecs and a time scale of a few tens of millions of years, greatly favors the production of massive stars (O7-B3)

over low-mass stars when compared to a canonical IMF, but not the production of stars of the highest mass (O4-O6), and completely terminates after a few tens of millions of years. The three star-formation hypotheses we have just discussed would each seem to meet these constraints equally well.

In assessing our "age" map it must be kept in mind that the "ages" we derive rest on the assumption that star formation is proceeding in the OB associations we map with a roughly power-law IMF, although the power-law exponent need not be very similar to the one we assume. It may be, however, that star formation in the arms has a mass function that is not even remotely similar to a power law. Consider the extreme example of delta-function IMF's: all star formation at a given location occurring at a single mass which is different at different locations. In this case it is obvious that our so-called "age" map would have nothing to do with the ages of the associations we observe, except to set an *upper bound* on the age of a given association. If this were so, it would not affect the constraint provided by the absence of star-formation sites between the arms, but it would of course greatly affect the interpretation of the star formation observed in the arms.

g) The Pattern Speed

The distribution and age distribution of the star clusters within the arms of M83 are essentially random. However, assuming that our age scale is approximately correct, the fact that so many stars formed within the last 50–80 million yr are seen, still entirely confined to the arms, places an interesting constraint on the "pattern speed," on the hypothesis that the initial trigger of the star formation associated with the arms is rigidly rotating perturbation. (This seems difficult to dispute since these inner arms are so obviously connected to the ends of the bar.) Since the entire rotation period of the galaxy is only ~ 60 million yr at the ends of the bar and ~ 75 million yr at the ends of the inner arms, the confinement of stars as old as 80 million yr to the close vicinity of the youngest stars we observe in the arm implies that the difference between the pattern velocity and the material velocity must be very slight. If the corotation radius lies at the ends of the inner arms, at a radius of about 180", the effective rotation period of the material in the arms relative to the pattern ranges upward from ~ 180 million yr at the ends of the bar. Within the constraints of this paragraph, this is a barely tenable choice for corotation; any larger radius is not. This choice for corotation yields $\Omega_p \sim 67 \text{ km s}^{-1} \text{ kpc}^{-1}$.

This determination of Ω_p , however, is strikingly different from the conclusion of Talbot (1980) that $\Omega_p \sim 26 \text{ km s}^{-1} \text{ kpc}^{-1}$. The two values are derived from totally different considerations. The lower value was derived by ascertaining the radius where the star-formation rate drops to zero and invoking the notion that the rate might be proportional to $\Omega - \Omega_p$. The higher value is derived from the lack of significant drift of young stars using the idea that such drift would be proportional to $\Omega - \Omega_p$. The latter seems to be the assumption subject to the least uncertainty, and consequently the conclusion is that

the rate of star formation is *not* proportional to $\Omega - \Omega_p$ (to any positive power). If it is related to Ω_p at all, it seems to peak just inside $\Omega = \Omega_p$. The relationship $B \propto (\Omega - 26)$ found by Talbot (1980) outside of $\Omega \sim 67 \text{ km s}^{-1} \text{ kpc}^{-1}$ therefore presumably conveys information about how the wave amplitude or number of modes varies with radius.

h) The Initial Mass Function

It is possible from our data to make a direct estimate of the initial mass function for the star formation we observe in M83. We obtain this estimate from studying how the luminosity distribution of our "clusters" changes from one age bin to the next, in a given annulus. To deduce the IMF, we produced histograms of the quantity $B(0)$ mag "cluster," the blue extinction-corrected flux of the "cluster" component as mapped in Figure 8, as a function of cluster age and galactic radius. We used 10 million yr age bins in the range 0–100 million yr, 15" radius bins (like those of Table 1), and therefore constructed 120 histograms of cluster flux, using bins within each histogram of 25 of the flux units defined by TJD. Within each

annulus, we counted the number of pixels in the oldest age histogram (90–100 million yr) down to a limiting flux of 50 units [$\mu_B(\text{cluster}) = 23.25$], then tabulated the fluxes in each of the other age histograms in the annulus that corresponded to the same number of pixels brighter than that flux. The results, normalized to the sum of the flux values for the four age bins 20–60 million yr, are shown in Figure 11 for the annuli between 105" and 180". Inward of 105" the number of pixels per bin with recent star formation drops rapidly: one additional set of values was obtained by combining the data in the 60"–105" annulus, and this is also plotted in Figure 11. In addition, we have plotted in Figure 11 behavior of two theoretical IMF's with upper main-sequence exponents of 1.35 and 2.00, the Salpeter IMF and the Lequeux IMF.

The data in Figure 11 should reflect the properties of the initial mass function(s) of the most luminous clusters in M83. Statistical errors can be estimated by the small scatter between the data from the various annuli, which also serves to show how little this property of the IMF varies with radius in the galaxy, at least in this inner region. Even assuming that there actually exists a uniform

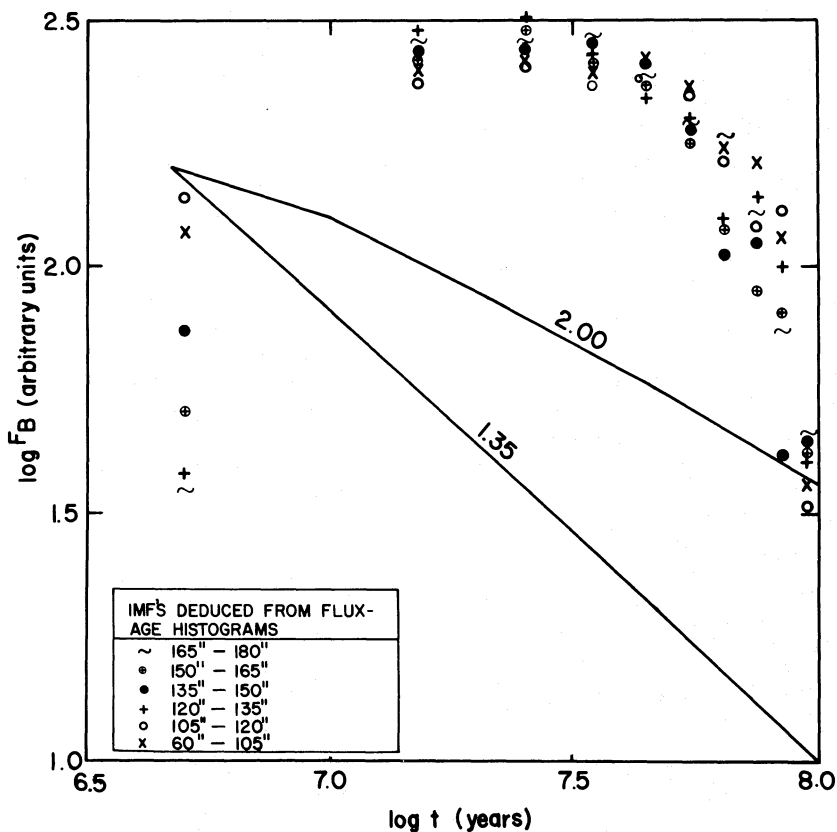


FIG. 11.—The logarithms of the mean luminosities of the brightest pixels ("cluster") in the radial ranges shown, as a function of their ages as deduced by the techniques of this paper. Also shown is the luminosity evolution of the two model initial mass functions used in this paper. The relative absence of luminous clusters younger than 10 million yr could be due to obscuration of these clusters by the clouds in which they have formed; the steepening of the luminosity decline at large ages could be due to dispersion of associations of stars into areas larger than a pixel. Finding the peak luminosity at an "age" as late as 30 million yr is surprising, and seems explicable only if a large fraction of the "clusters" make essentially no stars with effective temperatures greater than those corresponding to stars of $\sim 10 M_\odot$ with solar metallicity.

IMF in this galaxy, however, these data suffer from two possible severe systematic errors (in addition to possible systematic errors in the ages):

1. Many of the youngest clusters will undoubtedly be concealed by the dark clouds in which they have formed. This must account at least in part for the relatively low flux found for clusters younger than 10 million yr.

2. "Clusters" of stars that are not gravitationally bound when formed will disperse out of the pixel in which they are formed in a few million yr. Since the few sites containing the youngest stars we see in the galaxy ($t < \sim 5 \times 10^6$ yr) are typically 4–6 pixels across, this problem is perhaps not too severe, but it undoubtedly contributes to the steepening of the data in Figure 11 at the oldest ages.

The principal difficulty in understanding Figure 11, however, is not connected with either of these systematic errors. The principal problem is the broad peak in luminosity per cluster between the 30–40 million yr bins. It does not seem possible that any appreciable fraction of the young clusters could remain hidden in clouds for periods longer than 10 million yr, but this would be the only tenable explanation for such a delayed peak in the cluster luminosity in the context of uniformly populated power-law IMF's if our adopted age scale is correct. The position of the peak in Figure 11 suggests, therefore, that *a substantial fraction of the star formation we are measuring in M83 is proceeding with IMF's greatly deficient in stars with colors bluer than $8-10 M_{\odot}$ stars with $Z = Z_{\odot}$* . These data, in other words, provide support for the point of view already suggested that the IMF is truncated above $8-10 M_{\odot}$ unless the high Z greatly alters the colors of the most massive stars. If the IMF's are so truncated, then the "age map" in Figure 8 is instead a map primarily of the high-mass cutoff in the IMF as a function of position in the galaxy.

The various data supporting the hypothesis that the IMF in M83 is what we naively would call "peculiar" are summarized in the conclusions.

VI. CONCLUSIONS

By a combination of techniques utilizing color and morphological information and models of the evolution of groups of stars and of interstellar extinction, we have deconvolved the light of M83 into three populations:

1. A spheroidal population, with $M_v^0 \approx -17.5$, $(B - V)_0 = 0.87 \pm 0.05$, $(U - B)_0 = 0.31 \pm 0.05$;

2. An "old disk" population that dominates the light of the bar and the interarm region. This stellar disk has significant azimuthal structure at all radii, but our knowledge of the amplitude of the fluctuations is limited by uncertainty in the inclination of M83 and to a certain extent by uncertainty in the disk surface brightness in the arm regions;

3. A "young cluster" population that dominates the light of the arms. After subtraction of the disk, the remaining light in the arms can be readily understood as due to clusters and associations of stars with ages ranging from ~ 10 million to ~ 100 million yr, whose colors may

successfully be interpreted with models of cluster evolution and normal reddening.

The star formation in the inner arms of M83 has a number of remarkable properties which we have discussed in this paper:

1. The production of OB stars in the prominent associations along the arms is truly prodigious, a result that has also been obtained for some associations in M101 by other investigators. It follows that the production of less massive stars cannot be occurring at the same sites at a rate proportional to any power-law IMF resembling the IMF derived from the solar neighborhood, and that vigorous nucleosynthesis that should be associated with the massive stars we are observing must be largely disconnected from the conversion of gas mass into stars, which is generally dominated by the low-mass end of the IMF. Furthermore, the amount of nucleosynthesis implied by our observations, and its radial distribution, is ample to produce the observed radial abundance gradient in the gas.

2. The star formation we observe essentially fills the locus of the inner arms. If this is not merely the result of diffusion of the orbits of newly formed stars from a few sites of star formation, then the *sites* of star formation essentially fill the locus of the arms. When the gas density in this galaxy is mapped with high resolution, this will place constraints on the nature of the clouds forming stars.

3. The dramatic contrast between the arm locus essentially full of stars younger than $\sim 10^8$ yr and the interarm locus essentially empty of these stars provides strong constraints both on the star formation time scale and the difference between the material velocity and the spiral pattern velocity. However, there is no evidence for any "drift motion" or systematic variation of cluster age with azimuthal position in the spiral arms, except for an apparent tendency for the youngest associations and the H α flux to lie on the inner edge of the arm. What is evidently required to explain these observations is a star-forming mechanism that:

a) Globally triggers formation of massive stars in an accurate two-armed spiral-shaped pattern;

b) Locally acts in a largely stochastic way over a distance scale of a few hundred parsecs and a time scale of a few tens of millions of years;

c) Greatly favors the production of massive stars (O7–B3) over low-mass stars when compared to a canonical IMF, but not the production of stars of the highest mass (O4–O6);

d) Completely terminates after a few tens of millions of years.

Corotation of the pattern and the material must lie at the ends of the inner arms at $r \sim 180''$, yielding $\Omega_p \sim 67 \text{ km s}^{-1} \text{ kpc}^{-1}$.

4. The following evidence suggests variations in the IMF within M83 as well as variations from the mean solar-neighborhood IMF:

a) The distribution of H α does not match the distribution of the bluest patches in $U - B$;

b) The star formation rates at various radii estimated

from the H α are lower than those estimated from *UBV* colors, implying an IMF deficient in the highest mass stars relative to the Salpeter IMF (or possibly that the Lyman continuum of the highest mass stars is significantly weaker than for stars of comparable mass in the solar neighborhood);

c) The star-formation rates estimated both from H α and from *UBV* are greatly in excess of plausible rates of gas consumption, implying that these massive stars are forming out of proportion to the rate of formation of low-mass stars;

d) The distribution of the luminosities of the brightest clusters in M83 as a function of age peaks at ~ 30 million yr age. This result is explicable only if a large fraction of these bright clusters make no stars at all with $U - B$ colors corresponding to normal Population I stars more massive than $\sim 10 M_{\odot}$. This may truly be a truncation of the IMF at the high-mass end, or could possibly be due instead to blanketing in the envelopes and atmospheres of the massive stars sufficient to significantly lower their effective temperatures. In either case it provides an alternate explanation for the chaotic distribution of the "ages" in our age map.

Certainly one of the most important results of this paper is the evidence we have uncovered that the IMF in the arms of M83 cannot successfully be represented by a power law over the customary mass range with normal Population I stars. It should be possible to constrain the IMF further than we have been able to do here:

1. By comparison of the interarm colors to the total amount of star formation we have measured in the arms, it should be possible to put a constraint on the ratio of the production of high-mass stars to the production of stars whose main-sequence lifetimes are 100–200 million yr,

postulating the density-wave hypothesis and assuming that the star-formation rate in the arms of M83 has been much the same over the last several rotation periods of the inner part of this galaxy. This calculation requires careful modeling of the evolution of the interarm light and accurate dynamical information for the inner part of the galaxy, which, fortunately, should soon be available (Peterson 1981; Pence and de Vaucouleurs 1981).

2. By studying the color-luminosity evolution of improved models of OB stars, especially by incorporation of mass loss and the variations with metal abundances appreciably greater than solar, it should be possible to reduce the uncertainty in the absolute age assignments.

It is a pleasure to thank Charles Peterson for providing his velocity data in advance of publication. Once again, we would like to thank the staff of Cerro Tololo Inter-American Observatory for help with the observations, and the staff of Kitt Peak National Observatory for assistance and generous allocations of time on the IPPS, which was used extensively in the early stages of this work. We would also like to thank Don Johnson for help with the Rice Picture Processing System, with which this work was completed. Most of this work was carried out with the support of NSF grant AST 78-00924; the Rice Picture Processing System was supported by NSF grant ENG 77-02006 and ENG 78-11507. We thank the referee, Steve Strom, for numerous criticisms that greatly strengthened the presentation of our results. Finally, we thank George Simon and the Air Force Geophysics Laboratory for providing funds for color reproductions of Figures 8 and 9, which may be obtained by request to the first author.

REFERENCES

- Anthony-Twarog, B. J., Twarog, B. A., and McClure, R. D. 1979, *Ap. J.*, **233**, 188.
- Arnett, W. D. 1978, *Ap. J.*, **219**, 1008.
- Bash, F. N. 1979, *Ap. J.*, **233**, 524.
- Blitz, L., and Shu, F. H. 1980, *Ap. J.*, **238**, 148.
- Boroson, T. 1980, Ph.D. thesis, University of Arizona.
- Casse, M., Kunth, D., and Scalo, J. M. 1979, *Astr. Ap.*, **76**, 346.
- Combes, F., Encrernaz, P. J., Lucas, R., and Welichew, L. 1978, *Astr. Ap.*, **67**, L13.
- Contopoulos, G. 1979, *Photometry, Kinematics, and Dynamics of Galaxies*, ed. D. S. Evans (Austin: University of Texas), p. 425.
- Danvers, C.-G. 1942, *Ann. Obs. Lund*, No. 10.
- Davis, J. C. 1979, Ph.D. thesis, Rice University.
- de Vaucouleurs, G. 1964, in *IAU Symposium No. 20, The Galaxy and the Magellanic Clouds*, ed. F. J. Kerr and A. W. Rodgers (Canberra: Australian Academy of Science), p. 195.
- . 1970, in *IAU Symposium No. 38, The Spiral Structure of Our Galaxy*, ed. W. Becker and G. Contopoulos (Dordrecht: Reidel), p. 18.
- . 1979, *A.J.*, **84**, 1270.
- Dixon, M. E., Ford, V. L., and Robertson, J. W. 1972, *Ap. J.*, **174**, 17.
- Dufour, R. J., Talbot, R. J., Jr., Jensen, E. B., and Shields, G. 1980, *Ap. J.*, **236**, 119.
- Eggen, O. J. 1976, *Quart. J.R.A.S.*, **17**, 472.
- . 1977, *Pub. A.S.P.*, **89**, 187.
- Elias, J. H. 1978a, *Ap. J.*, **224**, 453.
- . 1978b, *Ap. J.*, **224**, 857.
- Elmegreen, B. G. 1979, *Ap. J.*, **231**, 372.
- Elmegreen, D. M. 1980a, *Ap. J. Suppl.*, **43**, 37.
- . 1980b, *Giant Molecular Clouds in the Galaxy*, ed. P. M. Solomon and M. G. Edwards (Oxford: Pergamon), p. 231.
- Evans, D. S. 1956, in *Vistas in Astronomy*, 2, ed. A. Beer (London: Pergamon), p. 1555.
- Faber, S. M., and Gallagher, J. S. 1979, *Ann. Rev. Astr. Ap.*, **17**, 135.
- Gerola, H., and Seiden, P. E. 1978, *Ap. J.*, **223**, 129.
- Greenstein, J. L., Neugebauer, G., and Becklin, E. E. 1970, *Ap. J.*, **161**, 519.
- Harris, G. L. H., and Harris, W. E. 1977, *A.J.*, **82**, 612.
- Heiles, C. 1980, *Ap. J.*, **235**, 833.
- Hoessel, J. G., and Melnick, J. 1980, *Astr. Ap.*, **84**, 317.
- Huntley, J. M. 1978, *Ap. J. (Letters)*, **225**, L101.
- . 1979, in *Photometry, Kinematics, and Dynamics of Galaxies*, ed. D. S. Evans (Austin: University of Texas), p. 483.
- . 1980, *Ap. J.*, **238**, 524.
- Iben, I. 1965, *Ap. J.*, **141**, 993 and **142**, 1447.
- . 1966, *Ap. J.*, **143**, 483, 505, and 516.
- . 1967, *Ap. J.*, **147**, 624 and 650.
- Israel, F. P., Goss, W. M., and Allen, R. J. 1975, *Astr. Ap.*, **40**, 421.
- Jensen, E. B. 1977, Ph.D. thesis, University of Arizona.
- Jensen, E. B., Strom, K. M., and Strom, S. E. 1976, *Ap. J.*, **209**, 748.
- Johnson, H. L. 1966, *Ann. Rev. Astr. Ap.*, **4**, 193.
- . 1968, in *Nebulae and Interstellar Matter*, ed. B. M. Middlehurst and L. H. Allen (Chicago: University of Chicago Press), p. 167.
- Kahn, F. D. 1974, *Astr. Ap.*, **37**, 149.

- Kerr, F. J. 1967, in *IAU Symposium No. 31, Radio Astronomy and the Galactic System*, ed. H. van Woerden (London: Academic), p. 239.
- Lada, C. J., Blitz, L., and Elmegreen, B. G. 1979, in *Protostars and Planets*, ed. T. Gehrels (Tucson: University of Arizona Press), p. 341.
- Larson, R. B. 1976, *M.N.R.A.S.*, **176**, 31.
- . 1977, in *The Evolution of Galaxies and Stellar Populations*, ed. B. M. Tinsley and R. B. Larson (New Haven: Yale University Press), pp. 110–111.
- Lee, T. A. 1970, *Ap. J.*, **162**, 217.
- Lequeux, J. 1979, *Astr. Ap.*, **80**, 35.
- Liszt, H. S., and Burton, W. B. 1980, *Ap. J.*, **236**, 779.
- Menzies, J. 1972, *M.N.R.A.S.*, **156**, 207.
- Mezger, P. 1978, *Astr. Ap.*, **70**, 565.
- Miller, R. H., and Smith, B. F. 1979, *Ap. J.*, **227**, 785.
- Morton, D. C., and Adams, T. F. 1968, *Ap. J.*, **151**, 611.
- Mouschovias, T. Ch., Shu, F. H., and Woodward, P. R. 1974, *Astr. Ap.*, **33**, 73.
- Mueller, M. W., and Arnett, W. D. 1976, *Ap. J.*, **210**, 670.
- Oort, J. H. 1974, in *IAU Symposium No. 58, The Formation and Dynamics of Galaxies*, ed. J. R. Shakeshaft (Dordrecht: Reidel), p. 375.
- . 1977, *Ann. Rev. Astr. Ap.*, **15**, 295.
- Panagia, N. 1973, *A.J.*, **78**, 929.
- Parker, E. N. 1966, *Ap. J.*, **145**, 811.
- Pence, W., and de Vaucouleurs, G. 1981, in preparation.
- Peterson, C. 1981, in preparation.
- Peterson, C. J., Rubin, V. C., Ford, W. K., and Thonnard, N. 1978, *Ap. J.*, **219**, 31.
- Roberts, W. W., Jr. 1969, *Ap. J.*, **158**, 123.
- . 1979a, in *IAU Symposium No. 84, The Large-Scale Characteristics of the Galaxy*, ed. W. B. Burton (Dordrecht: Reidel), p. 175.
- . 1979b, in *Photometry, Kinematics, and Dynamics of Galaxies*, ed. D. S. Evans (Austin: University of Texas), p. 461.
- Roberts, W. W., Jr., Huntley, J. M., and van Albada, G. D. 1979, *Ap. J.*, **233**, 67.
- Robertson, J. W. 1971, *Ap. J.*, **170**, 353.
- . 1972, *Ap. J.*, **177**, 473.
- Rogstad, D. H., Lockhart, I. A., and Wright, M. C. H. 1974, *Ap. J.*, **193**, 309.
- Rots, A. H. 1975, *Astr. Ap.*, **45**, 43.
- Sandage, A., and Visvanathan, N. 1978, *Ap. J.*, **223**, 707.
- Sanders, R. H. 1977, in *Chemical and Dynamical Evolution of Our Galaxy*, ed. E. Basinska-Brzesik and M. Mayor (Geneva: Geneva Observatory), p. 103.
- Schweizer, F. 1976, *Ap. J. Suppl.*, **31**, 313.
- Scott, J. S., Jensen, E. B., and Roberts, W. W., Jr., 1977, *Nature*, **265**, 123.
- Scoville, N. Z., and Hersh, K. 1979, *Ap. J.*, **229**, 578.
- Searle, L. 1971, *Ap. J.*, **168**, 327.
- Searle, L., Sargent, W., and Bagnuolo, W. 1973, *Ap. J.*, **179**, 423.
- Seiden, P. E., and Gerola, H. 1979, *Ap. J.*, **233**, 56.
- Shields, G. A., and Tinsley, B. M. 1976, *Ap. J.*, **205**, 66.
- Shu, F. H. 1974, *Astr. Ap.*, **33**, 55.
- . 1978, in *IAU Symposium No. 77, Structure and Properties of Nearby Galaxies*, ed. E. M. Berkhuijsen and R. Wielebinski (Dordrecht: Reidel), p. 139.
- Shu, F. H., Milione, V., Gebel, W., Yuan, C., Goldsmith, D. W., and Roberts, W. W. 1972, *Ap. J.*, **173**, 557.
- Smith, L. F., Biermann, P., and Mezger, P. 1977, *Astr. Ap.*, **66**, 65.
- Solomon, P. M., and Sanders, D. B. 1980, in *Giant Molecular Clouds in the Galaxy*, ed. P. M. Solomon and M. G. Edwards (Oxford: Pergamon Press), p. 41.
- Spitzer, L. 1968, *Diffuse Matter in Space* (New York: Interscience), p. 85.
- Stetson, P. B. and Harris, W. E. 1977, *Ap. J.*, **82**, 954.
- Stothers, R. 1963, *Ap. J.*, **138**, 1074.
- . 1964, *Ap. J.*, **140**, 510.
- . 1966, *Ap. J.*, **143**, 91 and **144**, 959.
- Stothers, R., and Chin, C.-W. 1968, *Ap. J.*, **152**, 225.
- . 1977, *Ap. J.*, **211**, 189.
- Strom, S. E., Jensen, E. B., and Strom, K. M. 1976, *Ap. J. (Letters)*, **206**, L111.
- Strom, S. E., and Strom, K. M. 1978, in *IAU Symposium No. 77, Structure and Properties of Nearby Galaxies*, ed. E. Berkhuijsen and R. Wielebinski (Dordrecht: Reidel), p. 69.
- Talbot, R. J., Jr. 1977, in *Chemical and Dynamical Evolution of Our Galaxy*, eds. E. Basinska-Greżesik and M. Mayor (Geneva: Geneva Observatory), p. 31.
- . 1980, *Ap. J.*, **235**, 821.
- Talbot, R. J., Jr., and Arnett, W. D. 1975, *Ap. J.*, **197**, 551.
- Talbot, R. J., Jr., Jensen, E. B., and Dufour, R. J. 1979, *Ap. J.*, **229**, 91 (TJD).
- Tinsley, B. M. 1972, *Astr. Ap.*, **20**, 383.
- Tully, R. B. 1974, *Ap. J. Suppl.*, **27**, 447.
- van der Laan, H. 1978, in *IAU Symposium No. 77, Structure and Properties of Nearby Galaxies*, ed. E. M. Berkhuijsen and R. Wielebinski (Dordrecht: Reidel), p. 145.
- Visser, H. C. D. 1978, Ph.D. thesis, University of Groningen.
- Visvanathan, N., and Sandage, A. 1977, *Ap. J.*, **216**, 214.
- Whitford, A. E. 1958, *Ap. J.*, **144**, 305.
- Woodward, P. R. 1976, *Ap. J.*, **207**, 484.
- Wray, J. D., and de Vaucouleurs, G. 1980, *A.J.*, **85**, 1.
- Yuan, C., and Grosbol, P. 1981, *Ap. J.*, **243**, 444.

REGINALD J. DUFOUR and RAYMOND J. TALBOT, JR.: Department of Space Physics and Astronomy, Rice University, Houston, TX 77001

ERIC B. JENSEN: The Aerospace Corporation, Mail Station A2/1251, P.O. Box 92957, Los Angeles, CA 90009

PLATE 12

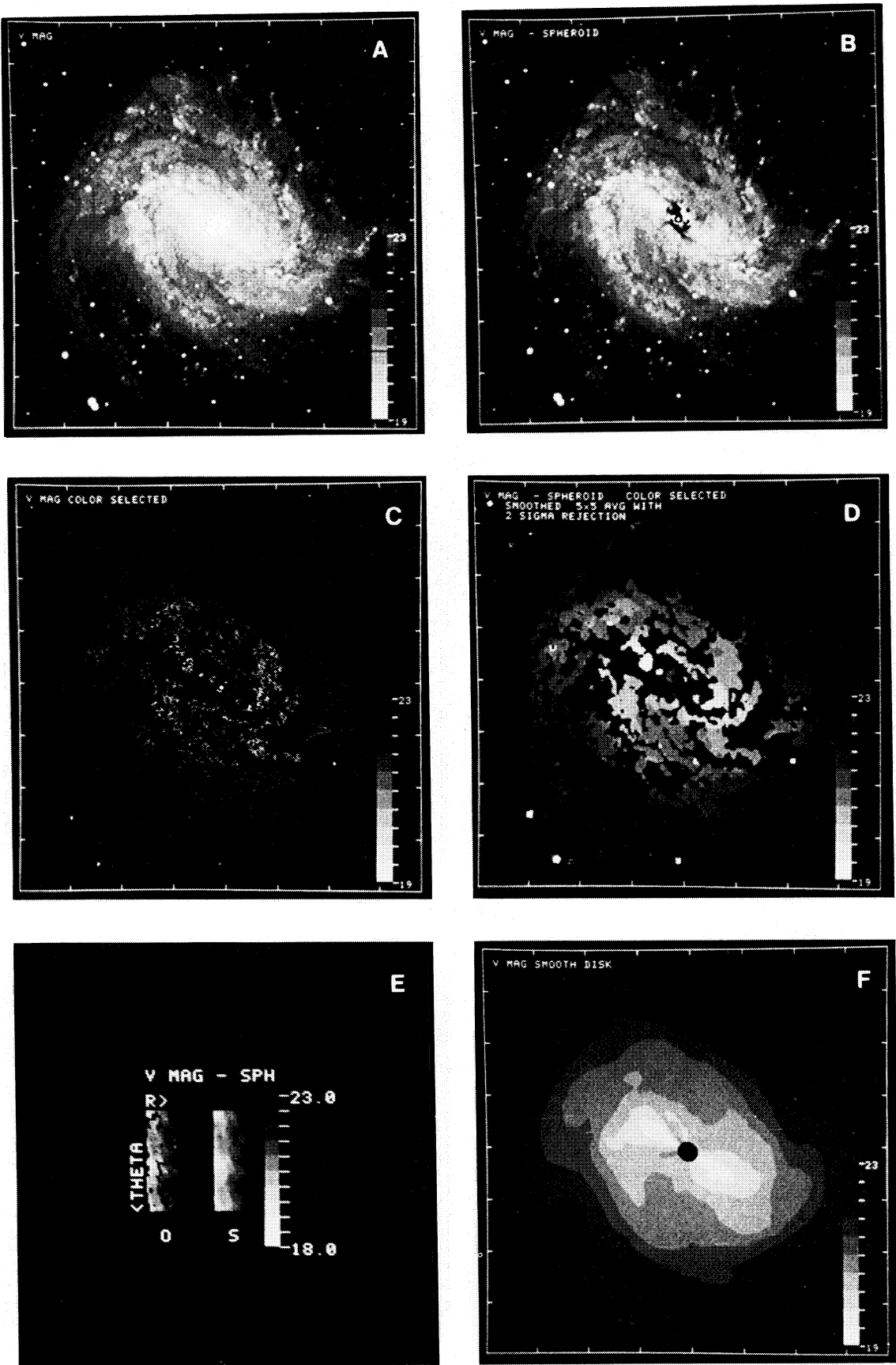


FIG. 2

JENSEN, TALBOT, AND DUFOUR (see p. 719)

© American Astronomical Society • Provided by the NASA Astrophysics Data System

PLATE 13

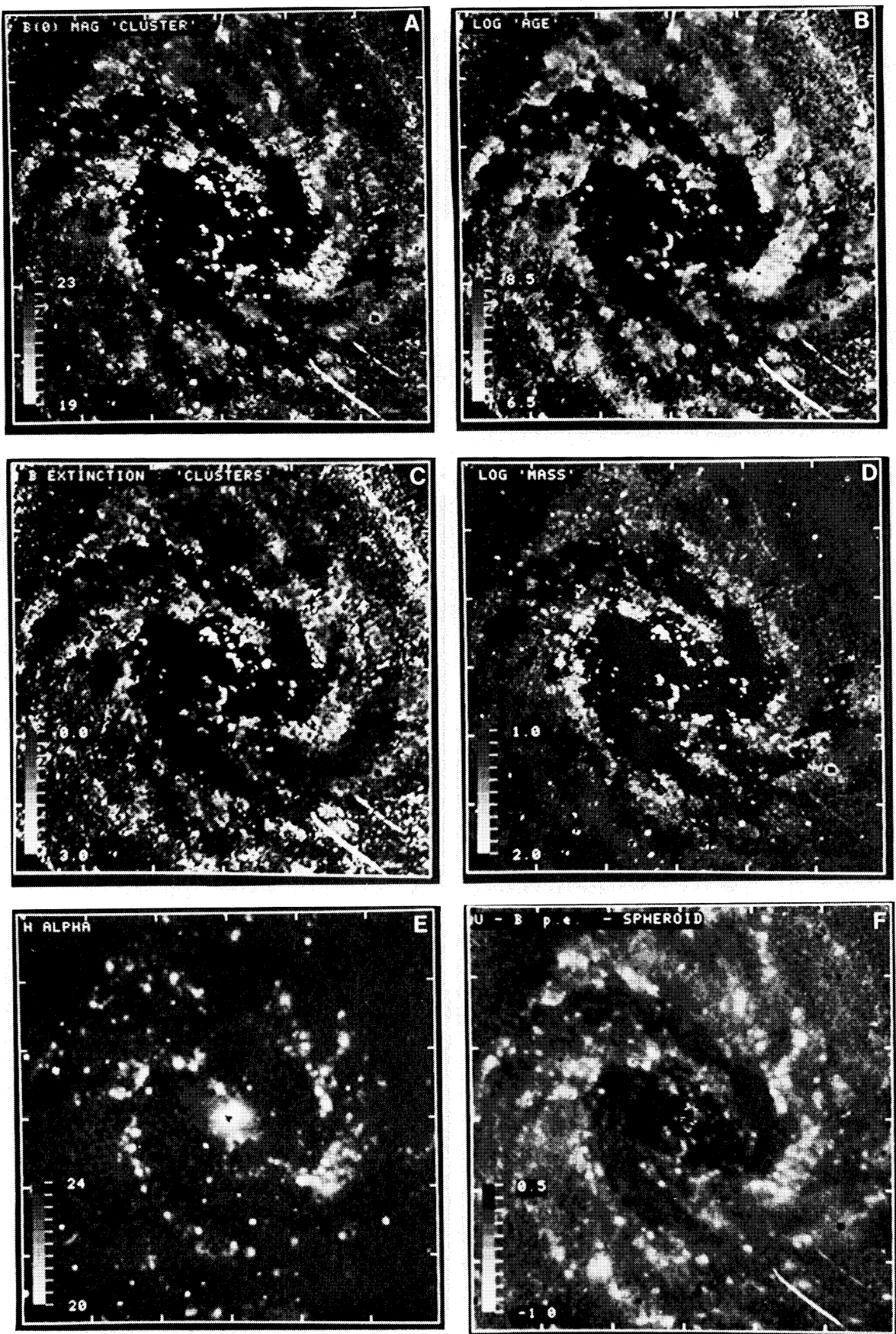


FIG. 8

JENSEN, TALBOT, AND DUFOUR (see p. 723)

© American Astronomical Society • Provided by the NASA Astrophysics Data System

PLATE 14

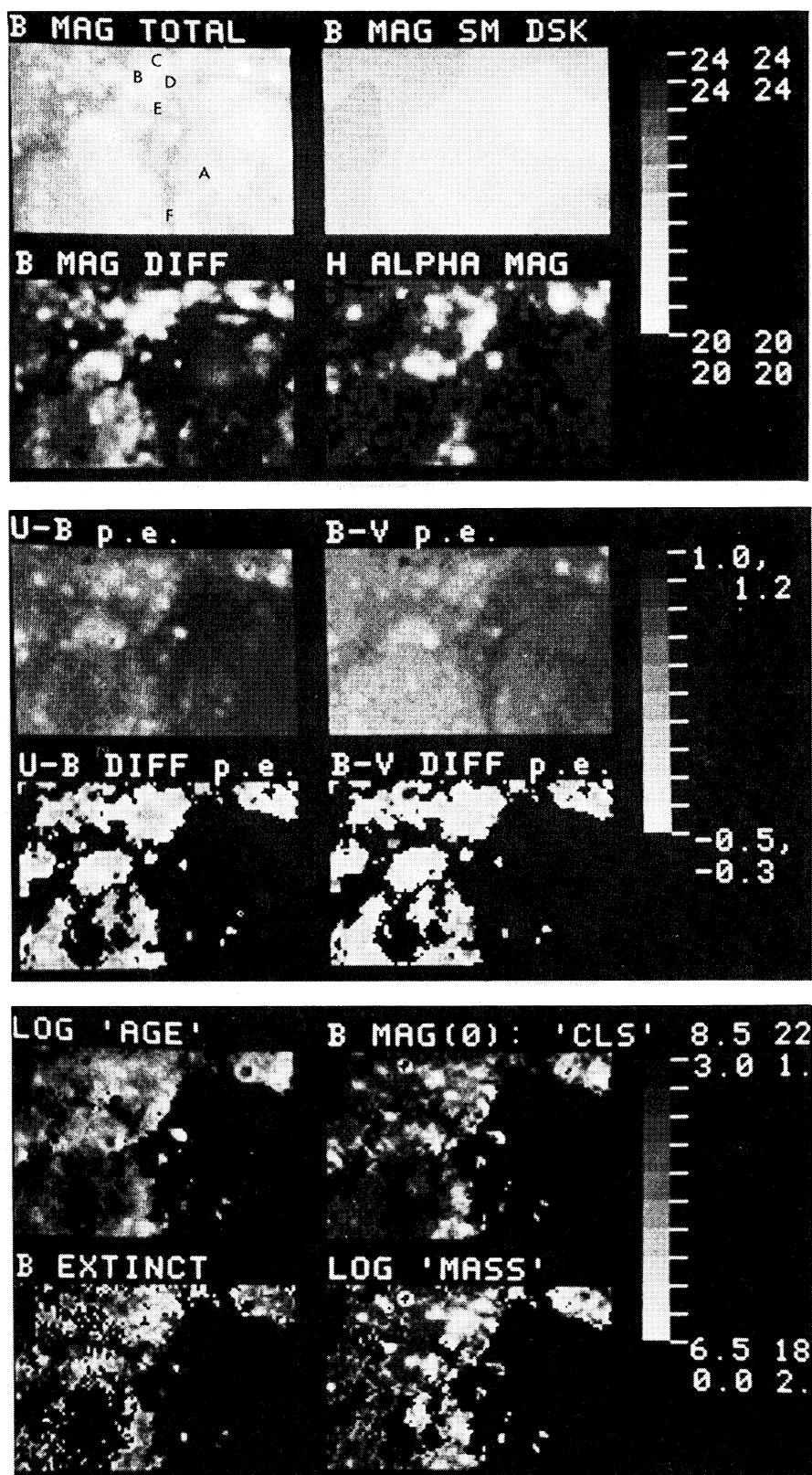


FIG. 9

JENSEN, TALBOT, AND DUFOUR (see p. 723)